Universidad de Sevilla
Escuela Técnica Superior de Ingeniería

Local Plasticity Modelling Around a Stress Concentration Using the Distributed Dislocations Method

Master thesis presented by
Neven Mahmoud Hussein Mostafa Darwish,
Submitted to the Departamento de Ingeniería Mecánica y Fabricación
of Universidad de Sevilla
to obtain the degree of Máster en Diseño Avanzado en Ingeniería Mecánica.

Supervised by
Dr. Alfredo Navarro Robles

Seville, November 2016.

Universidad de Sevilla
Escuela Técnica Superior de Ingeniería

Modelado de plasticidad local alrededor de una concentración de tensiones utilizando un método de dislocaciones distribuidas

Memoria realizada por
Neven Mahmoud Hussein Mostafa Darwish,
presentada ante el Departamento de Ingeniería Mecánica y Fabricación de la Universidad de Sevilla
para la obtención del Grado de Máster en Diseño Avanzado en Ingeniería Mecánica.

Dirigida por
Dr. Alfredo Navarro Robles

Sevilla, Noviembre 2016.

Acknowledgements

I would like to express my appreciation to my advisor: Dr. Alfredo Navarro Robles. Thanks for giving me the opportunity to be part of your research group and for the continuous support of my study. I learned a lot from you and I hope that our collaboration continues in the future. My thanks also goes to Dr. Victor Chaves Repiso for being there to answer my questions.

Also, thanks to the Ministry of Education, Culture and Sport of Spain for making this study possible by providing its funding to me. My gratitude also goes to my colleagues in the Master program especially to Gabriel who always had the time to help no matter how busy he was.

Thanks to my friends in Spain and Egypt. The most special thanks goes to my family especially to my father and my mother for being such a big source of supporting and encouragement, if it weren't for you, I couldn't have been here. I'd like to express my best gratitude to my beloved husband who has always been supporting and encouraging me. Your support means a lot to me.

Contents

Chapter 1

Introduction

In engineering components subject to external stresses, local plasticity at stress concentrations has always been a concerning issue as it may lead to failure. Examples of the stress raising features include holes, notches, sharp edges, grooves and keyways. Researchers have been introducing methods in order to improve the modelling of local plasticity. While designing a component containing stress raising features and subject to stresses, the stress state arising in the neighborhood of the stress raiser needs to be determined in order to avoid undesirable local yielding of components. Different methods for local plasticity analysis at stress concentrations will be discussed briefly. One method is to make an elastic stress analysis of the component and then to determine the cyclic plastic behavior by calculating the local strain state analytically using the methods of Neuber [1] or Glinka [2]. Although these methods are economic and fast to be done, however, they have the inconvenience that they do not give an exact solution and cannot predict local strain history. Another method is to make an elastic-plastic

finite element analysis of the component over a number of load cycles. While this method is precise to a great extent and can predict the local stress-strain history, it requires a lot of computation capability as it does not take into account that the component is mostly elastic during the calculation process.

An improved method have been proposed by Blomerus and Hills [3] in order to model local plasticity efficiently. This method employs stationary edge dislocations at the positions where yielding is expected to occur to simulate plasticity. This method shows good agreement with the results from the finite element (FEM) analysis and at the same time, is easy to be applied. Another method outlined by Mura [4] is similar to the method proposed by Blomerus and Hills. The method proposed by Blomerus and Hills can be applied to elastic-perfectly plastic materials and takes into account the redistribution of stresses that accompanies plastic flow, while on other hand, the method outlined by Mura is only applied to perfectly plastic materials and does not take into consideration the redistribution of stress.

The research group of Professor Alfredo Navarro in the Department of Mechanical Engineering and Manufacturing has been using dislocation models of short crack growth for many years now in order to account for the interaction between cracks and microstructural barriers to plastic slip such as grain boundaries.

Building upon the classical work of Bilby, Cottrell and Swinden on the representation of a crack and its associated plastic zones by means of dislocations [5], Navarro and de los Rios initially developed a model for fatigue microcracks growing in plain infinite bodies [6]. It was assumed that plastic displacement

takes place in rectilinear slip bands cutting across the grains of the material. The simplification of reducing the crack and the plastic zones to a single line seems appropriate in the early stages of fatigue failure under uniaxial loading since it is now well-known that the fatigue limit in metallic materials is a threshold condition for the propagation of short cracks growing within a few grains. Experimental evidence has shown that in plain specimens subjected to uniaxial loads near the fatigue limit cracks form on persistent slip bands and grow along them. Thus, it makes sense to consider that dislocations are constrained (e.g. by stacking fault energy) to remain on their original planes and pile up against grain boundaries, giving rise to rectilinear slip bands extending through the first few grains. The microcrack nucleates in the grain which presents the most favorable size and crystallographic orientation for the formation of persistent slip bands. Within the first grain, the plastic zone spreads from the crack tip to the first microstructural barrier (e.g. the grain boundary), where it will be stopped until the local stress at the barrier is high enough for activating plastic slip in the following grain. The calculation of the stress acting upon the barrier is thus of fundamental importance in this framework. It can be shown that it depends on the applied stress and on the relative position of the crack tip with respect to the barrier, in such a way that the nearer the crack tip is to the barrier, the higher the stress acting upon it is. The fatigue limit is the threshold applied stress below which plastic slip in the next grain will not be activated even when the crack itself reaches the boundary. In this case, the crack becomes non-propagating. If, on the other hand, the applied stress is above the fatigue limit, plastic slip will be promoted in the following grain once the crack tip is sufficiently close to the barrier. In this case, the process of spreading up to the next grain and

blocking is repeated at every successive grain. Thus the plastic zone is thought to grow in jumps. An oscillating crack propagation rate with smaller and smaller oscillations is predicted, which seems to be in agreement with the experimental evidence.

These Microstructural Fracture Mechanics models have been quite successful in explaining all known features of short fatigue cracks in the early stages of propagation. As it is has been stated above, these models rely heavily upon the assumption that both the crack and the associated plastic zones remain in the same (rectilinear) slip band. Now there are a number of important practical situations where this critical hypothesis may not apply. That would be the case for example of specimens subject to biaxial out-of-phase loads, where the rotation of the principal components of stress and strain may almost certainly result in plasticity being smeared in two-dimensional regions, as opposed to the case on in-phase loading where dislocations are more likely to remain in the maximum shear planes.

Another case of interest arises when studying notched components subjected to low-cycle fatigue, where the influence of the plastic zone associated with the notch itself, aside from the one associated with the propagating crack, is of high importance. The notch plastic zone is a bidimensional region even when the load acting upon the specimen is uniaxial.

Thus there is a lot of interest in our group in being able to model biaxial plastic zones (and their interaction with the microstructure). The present study represents a first step in this direction. We wanted to learn how to deal with the additional dimension and we chose a problem which seemed tractable in the

short span of time available for a Master's thesis and that could also be contrasted with continuum solutions readily obtainable too in a straight forward manner, such as a simple FEM model. We decided to implement the procedure proposed by Blomerus and Hills to describe the plastic zone created around a circular notch subjected to remote tension. We were, in particular, very much interested in their way to cope with the yield criterion and the plastic flow rule, i.e. we wanted to understand fully how these macroscopic concepts translate into the microscopic modeling by means of dislocations. On the other hand, it is not at all clear how the microstructure of the material may be brought in at the present stage of our investigation.

I would like to start this work with one of the simpler examples of the use of distributed dislocations to model plastic zones, namely the famous model of Bilby, Cottrell and Swinden for the plastic zones of a crack in an infinite medium. Consider a crack situated in the region $-a < x < a$ in an infinite body subjected to mode II loading. The plastic zone is situated at the ends of the crack in the linear regions $-c < x < -a$ and $a < x < c$. As shown in Figure 1.1, the crack and the plastic zones are modeled by a continuous distribution of infinitesimal edge dislocations whose Burgers vectors are in the x direction. The stresses, σ_1 and σ_2 represent the friction stress, σ_f, in the crack and the plastic zone respectively. The friction stress on the crack σ_1 is assumed to vanish if the crack faces are not in contact. When the plastic zone extends to a sufficient number of grains, the friction stress on the plastic zone σ_2 is considered equal to the elastic limit.

The equilibrium of dislocations is determined by an integral equation of the Cauchy type [5, 7]. The equation would be the same for the case of loading in

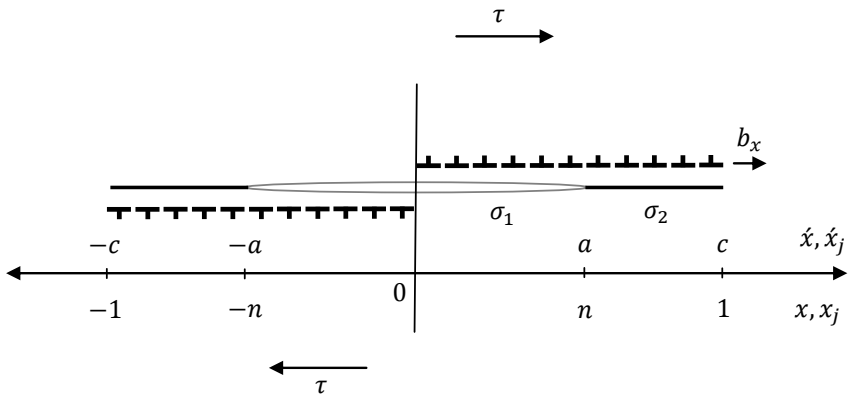

Figure 1.1: Representation of a crack and the crack tip plastic zone by edge dislocations.

mode III and I. The integral equation normalized with respect to c, in terms of the dimensionless coordinates $x = \acute{x}/c$ and $x_j = \acute{x}_j/c$, is as follows:

$$A \int_{-1}^{1} \frac{f(x_j)dx_j}{x - x_j} + (\tau - \sigma_f) = 0 \tag{1.1}$$

Where $f(x_j)$ is the dislocations distribution function that gives the number of dislocations between x_j and dx_j, τ is the applied shear stress and A is a constant for which $A = \mu b/2\pi$ for screw dislocations or $A = \mu b/2\pi(1 - \nu)$ for edge dislocations, where μ is the shear modulus of the material, b is the dislocation Burgers vector and ν is Poisson's ratio. The first term in the equation represents the sum of the stresses produced due to the interactions between the dislocations. Meanwhile σ_f is the friction stress that opposes the motion of dislocations in the crack and the plastic zone, taking values of σ_1 and σ_2 respectively.

This integral equation whose unknown is the dislocations distribution function $f(x_j)$ has an exact solution and can be solved analytically by the inversion

theory of Muskhelishvili [8]. There are two different solutions for the dislocation distribution function $f(x_j)$ depending on whether it is considered bounded or unbounded at the ends of the plastic zones [8, 7].

As the dislocations distribution function is bounded at both ends, it has the following expression [6]:

$$f(x_j) = \frac{\sigma_f}{\pi^2 A}\left[\cosh^{-1}\left(\left|\frac{1-nx_j}{n-x_j}\right|\right) - \cosh^{-1}\left(\left|\frac{1+nx_j}{n+x_j}\right|\right)\right] \tag{1.2}$$

Where $n = a/c$. There is an existence condition for the bounded solution which is as follows:

$$n = \cos\left(\frac{\pi}{2}\frac{\tau}{\sigma_f}\right) \tag{1.3}$$

As the distribution function is bounded at the ends of the plastic zones, this solution is possible only when the applied stress τ is lower than the friction stress opposing the movements of dislocations, i.e. $\tau < \sigma_f$.

In the procedure proposed by Blomerus and Hills, in order to calculate the strength and direction of Burgers vector for each dislocation, two requirements should be met. The first is that the net stress state should lay on the yield surface; and the second is that the flow direction must obey the associated flow rule, i.e. the normality condition on the yield surface. In the BCS model, the flow rule is automatically satisfied, as the dislocations that model the plastic zone are aligned with the slip bands emanating from the crack. Also in the BCS model, the friction stress is used for the equation of equilibrium of dislocations, while in the model of Blomerus and Hills, the yield stress is used.

This thesis applies the model proposed by Blomerus and Hills [3] to an infinite

plate containing a circular hole and subject to uniaxial remote tension in order to predict the yielded zone. The base idea of the method applied is to distribute stationary dislocations in the neighborhoods of the stress raising feature to predict the plastic zone of an elastic-perfectly plastic material under plane strain conditions. The dislocations distributed have similar properties as the edge dislocations in order to form a perturbation on the elasticity solution to a problem. The circular hole is implicitly included in the formulation by using specialized kernels; hence the efficiency of the procedure is improved.

Chapter 2

Description of the procedure

2.1 Introduction to the procedure

The method of Blomerus and Hills [3] has its idea developed from an analysis of crack tip plasticity concept of the BCS model [5]. Only plane strain conditions have been considered resulting to zero out-of-plane strain. Therefore the analysis of local plasticity is a plane strain one.

According to Blomerus and Hills, when analyzing crack tip plasticity, the maximum shear stress is aligned along rays that make an angle of about ±70.5° with the crack plane line. The plastic flow is customary assumed to happen only along these rays. These rays represent the plastic zone area collapsed on to a line. The directions of the dislocations Burgers vectors are assumed to be aligned along these rays. This results in the following integral equation:

$$\int_{ray} \left[\sigma^{d}_{xy}(x, x_j) + \sigma^{d_{im}}_{xy}(x, x_j)\right] B_x(x_j) dx_j + \tilde{\sigma}_{xy}(x) = k \tag{2.1}$$

Where $B_x(x_j)$ is the density of active dislocations and is equivalent to $\partial b_x/\partial x$ where b_x is the Burgers vector of a single dislocation, $\tilde{\sigma}_{xy}(x)$ is the accumulated stress along the ray, k is the yield strength of the material in shear, which is equal to $\sigma_Y/2$ according to Tresca's yield criterion or equal to $\sigma_Y/\sqrt{3}$ according to von Mises yield criterion, σ_{xy}^{d} is the stress resulting due to a single dislocation and $\sigma_{xy}^{d_{im}}$ are the image terms resulting from the symmetry conditions and the requirements that no traction stresses are present along the faces of the crack. The x-y is a right-handed Cartesian coordinate system with its x axis aligned with the direction of the ray.

The dislocation density at any position and the length of the plastic line can be found using equation (2.1) where a bounded solution is to be found, as the transition between the elastic and plastic stress states is smooth at the tip of the plastic line. By plotting the yield parameter contours normalized with respect to the yield stress of the material at some load level, a small and finite zone of plasticity where the yield condition is exceeded can be observed as shown in Figure 2.1 (a). This means that the assumption that plastic flow happens along a single line is just an approximation and the model needs to be improved.

To improve the modelling of the plastic flow, we need to modify the orientation of the distributed dislocations according to their physical meaning. Therefore we need to study the physical meaning of an edge dislocation [9]. To create a dislocation in two dimensions, a slit is made in an infinite body from the core of the dislocation to any infinitely remote point. The trajectory of this slit may take any form, and the formation of the dislocation is achieved by the imposition of constant displacement between adjacent points positioned at both side of the

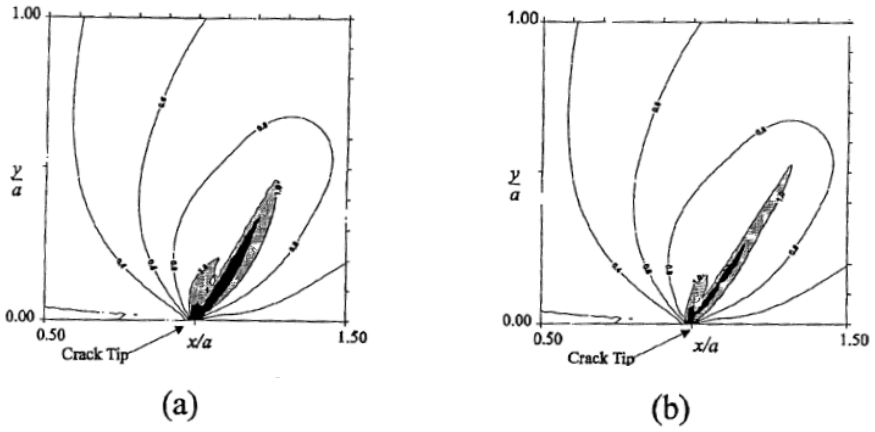

Figure 2.1: Yield contours for the model of inclined strip yield of crack tip plasticity with dislocations aligned with (a) ray and (b) slip directions [3].

slit, and then by the insertion or removal of material as necessary, and finally by welding the material back together. The imposed constant relative displacement is called the Burgers vector. Edge dislocations are used for the plane problems, where the Burgers vectors are located in the plane. The stress state induced by the dislocation depends on the Burgers vector components b_x and b_y, whereas it does not depend on the path cut taken.

There are two ways for an edge dislocation that has a Burgers vector component b_x to be created: by an opening displacement "climb" as shown in Figure 2.2 (a) and by a tangential displacement "glide" as shown in Figure 2.2 (b). In the first case, a cut is made along the positive y-axis, material is pulled apart, and then a thin strip of thickness equivalent to b_x is added before rejoining. In the second case, a cut is made along the positive x-axis and material slip occurs below the cut in the x-direction by an amount b_x before rejoining.

The meaning of the sign of the Burgers vector component b_x can be under-

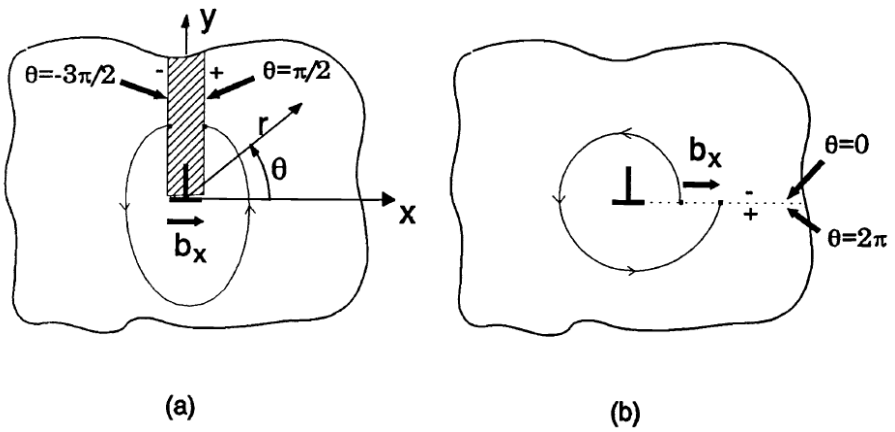

Figure 2.2: Creation of an edge dislocation (a) by an opening displacement "climb" or (b) by a tangential displacement "glide" [9].

stood by starting from the core of the dislocation and walking along the cut, hence we can differentiate between the positive side (+) on the right, and the negative side (−) on the left as shown in Figure 2.2 [10]. We need to differentiate between the "climb" dislocation and the "glide" dislocation. If the Burgers vector is perpendicular to the path cut, hence a strip is to be added as shown in Figure 2.2 (a), then the dislocation is called a "climb" one. If the Burgers vector is parallel to the path cut, hence shear displacements are present as shown in Figure 2.2 (b), then the dislocation is called a "glide" one, and the "glide plane" is defined by the path cut. In the present model, glide dislocations will be used to model plasticity.

Returning to the problem of crack tip plasticity, Figure 2.3 shows how an edge dislocation is generated. A cut is made along the glide plane from the core of the edge dislocation to infinity. Material is displaced in a shear sense by an amount b_x along both sides of the cut line. Hence, the increment of plastic flow can be represented macroscopically by material slip due to dislocations. This slip

of material occurs along the direction of the maximum shear stress under plane strain conditions by either Tresca or von Mises yield criterion.

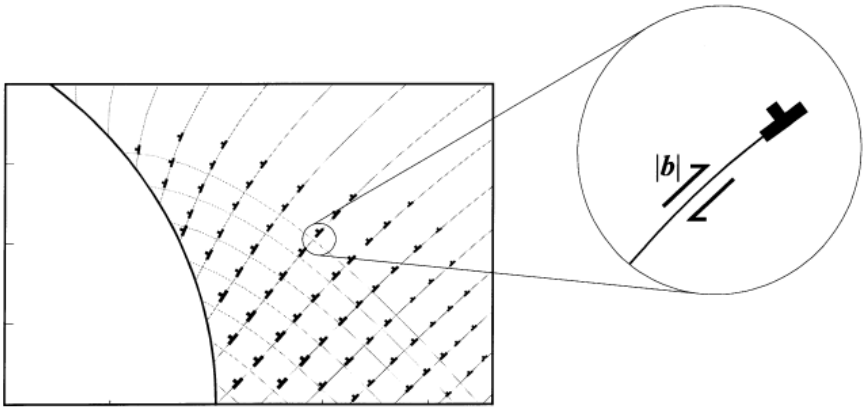

Figure 2.3: Representation of an increment in plastic flow by a distribution of edge dislocation [3].

Hence the modelling of the crack tip plasticity problem can be improved by aligning the dislocations Burgers vectors at each dislocation insertion point with the potential slip direction; i.e., the maximum shear stress direction. Figure 2.1 (b) shows the corresponding yield contours and it is obvious that the zone where the yield condition is exceeded is smaller, hence the solution is improved. Equation (2.1) is reformulated to take this into consideration and then an iterative method can be used in order to solve the problem.

The procedure has now been developed and can be applied for solving many problems with local plasticity present. The procedure models plastic flow of the material by distributing stationary dislocations. To demonstrate the model, the problem of a circular hole in an infinite plate subject to uniform tension will be analyzed.

2.2 Procedure outline

In the present model, glide dislocations will be used to model local plasticity in the neighborhood of an infinite plate containing a circular hole. The increase of plastic flow in a region can be represented by a continuous distribution of edge dislocations with their Burgers vectors aligned with the direction of the instantaneous maximum shear stress and also with their branch cuts following the trajectories of this stress.

The edge dislocations used in this model have similar physical properties as a crystallographic defect but they are used in a different way. In a crystallographic material, plastic flow is produced by the motion of dislocations through the material, while in this procedure, stationary dislocations are used.

A plasticity problem will now be considered from the continuum viewpoint. The material is assumed to have an elastic-perfectly plastic stress-strain curve, without work hardening and with a stress concentration in the component produced from this material. An increase in the load is made until reaching the elastic limit, when yielding first occurs, and then the load is increased more by a small amount. After the load exceeds the elastic limit, an elasticity solution can be applied approximately, and a small plastic zone is predicted at the stress concentration. By determining the stress contours where the yield condition has been exceeded, the extent of the plastic zone can be calculated. Dislocations are distributed in the plastic zone, at the positions where the yield condition has been exceeded, in order to bring back the stress state onto the yield surface. To calculate the strength and direction of Burgers vector for each inserted dislocation, two requirements should be met. The first is that the net stress state should lay on the

yield surface; and the second is that the flow direction must obey the associated flow rule, i.e. the normality condition on the yield surface. The distribution of such dislocations is made to form a perturbation on the elasticity solution to the problem to be studied. Thus, the stress raising feature is implicitly taken into account, and efficiency of the procedure is improved.

A small overall change in the stress state will be produced due to the distribution of dislocations, which is shown macroscopically as the redistribution of stress that occurs along with plasticity. As stress redistribution occurs, a shift in the trajectories of the maximum shear stress and accordingly in the preferred slip direction may occur, and the directions of Burgers vectors must be modified; because in accordance with the flow rule, they must always be aligned with the direction of the instantaneous maximum shear stress. Therefore, we need to take into consideration this redistribution of stress to get an accurate solution.

A small increase in the applied load will be made, and consequently a small increase in the plastic zone, where the yield condition is exceeded, will occur. This increment of plastic flow requires an additional distribution of dislocation to represent it, where the two criteria mentioned before should be satisfied, in addition to inserting dislocations at the positions from the previous load step. To calculate the instantaneous resultant total stress, we must take into account the current elastic solution in addition to the linear combination of all the active dislocations inserted in all previous load steps, which must satisfy the yield criterion. This procedure should be repeated each load step until convergence happens. The contributions of the inserted dislocations at each load step to the total Burgers vectors at each dislocation insertion point is stored, and therefore

there is be no need to use moving dislocations.

The degree of the loading non-proportionality determines the load increment size. Small load step are needed in case that the stress vectors in terms of stress-space is moving around the yield surface by large amounts; because the direction of the shear stress is assumed to remain constant during each load step and thus divergence will occur as a result of a very large load step. However, very large load steps can be used in the case of a nearly proportional loading.

2.3 Problem formulation

Because of symmetry, only the first quadrant is considered in modelling the plasticity. An array of probable dislocation sites was set up in the vicinity of the expected plastic zone as shown in Figure 2.4. A set of pseudo squares was formed by forming the array from a set of radial lines at w angular spacing, and a set of circular arcs arranged at rw radial spacing, where r is normalized to the radius of the hole, a, while maintaining an aspect ratio equal to 1 : 1 for the array. The strengths of the dislocations are found by collocating at the positions between the dislocations insertion points, as these collocation points cannot coincide with the dislocations insertion points because of the singular stresses at the dislocations insertion points.

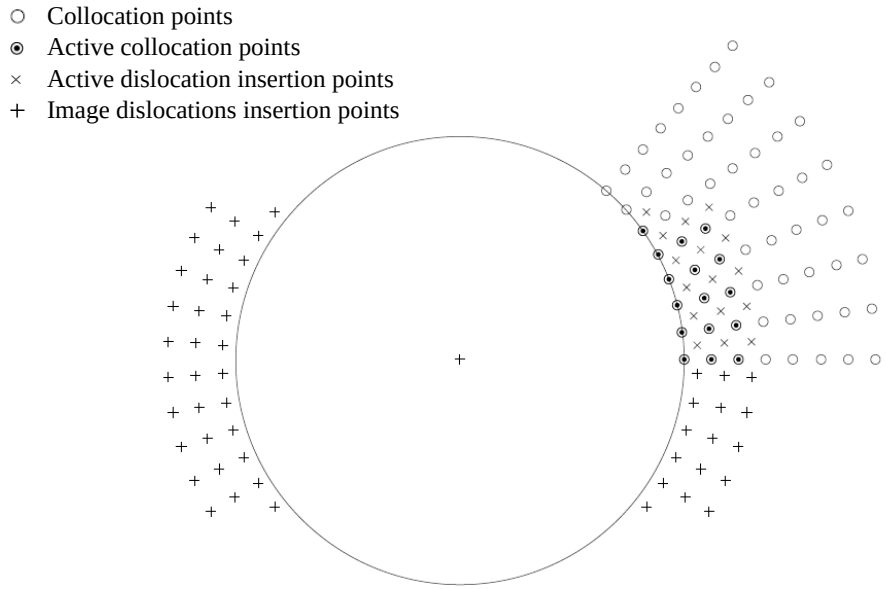

Figure 2.4: Discretization of the plastic zone.

The elastic stress state induced in an infinite plate containing a circular hole

under uniaxial remote tension, σ_0, in the polar coordinate system shown in Figure 2.5, is given by Timoshenko and Goodier [11] and is of the form:

$$\sigma_{rr}^{elastic} = \frac{\sigma_0}{2}\left(1 - \frac{1}{r^2}\right) - \frac{\sigma_0}{2}\left(1 + \frac{3}{r^4} - \frac{4}{r^2}\right)\cos 2\theta \tag{2.2}$$

$$\sigma_{\theta\theta}^{elastic} = \frac{\sigma_0}{2}\left(1 + \frac{1}{r^2}\right) + \frac{\sigma_0}{2}\left(1 + \frac{3}{r^4}\right)\cos 2\theta \tag{2.3}$$

$$\sigma_{r\theta}^{elastic} = \frac{\sigma_0}{2}\left(1 - \frac{3}{r^4} + \frac{2}{r^2}\right)\sin 2\theta \tag{2.4}$$

Where the radial coordinate has been normalized by the hole radius, a.

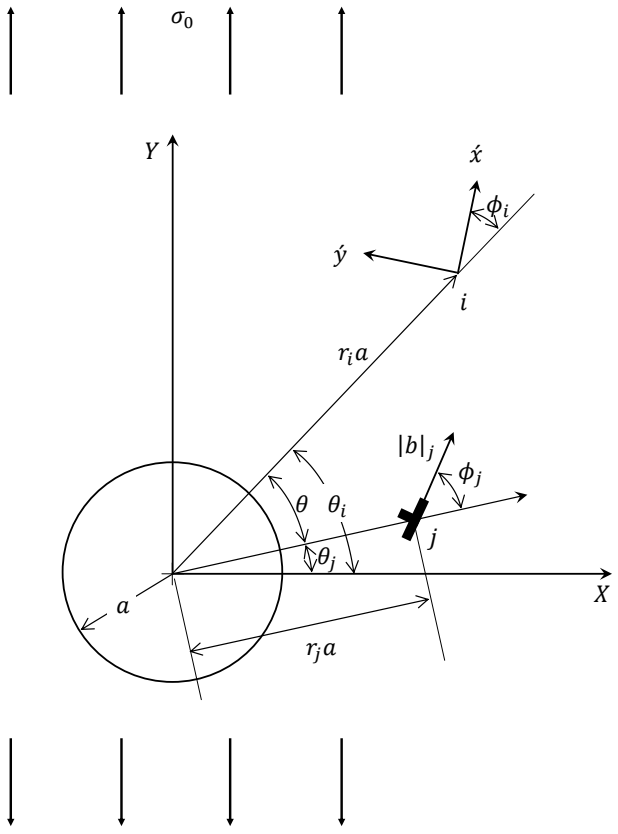

Figure 2.5: Infinite plate containing a circular hole and subject to remote tension σ_0.

The stress state induced in an infinite plate containing a circular hole at a field point, i, with position (r_i, θ_i) due to a single dislocation at a source point, j, with position (r_j, θ_j) whose Burgers vector components are b_x and b_y, calculated in its local coordinate system is given by Dundurs and Mura [12] and can be written as:

$$\sigma_{xx}^{d} = \frac{\mu}{\pi(\kappa+1)}\left[S_{xxx}\left(r_i,\theta_i,r_j,\theta_j\right)b_x + S_{yxx}\left(r_i,\theta_i,r_j,\theta_j\right)b_y\right] \tag{2.5}$$

$$\sigma_{yy}^{d} = \frac{\mu}{\pi(\kappa+1)}\left[S_{xyy}\left(r_i,\theta_i,r_j,\theta_j\right)b_x + S_{yyy}\left(r_i,\theta_i,r_j,\theta_j\right)b_y\right] \tag{2.6}$$

$$\sigma_{xy}^{d} = \frac{\mu}{\pi(\kappa+1)}\left[S_{xxy}\left(r_i,\theta_i,r_j,\theta_j\right)b_x + S_{yxy}\left(r_i,\theta_i,r_j,\theta_j\right)b_y\right] \tag{2.7}$$

Where μ is the modulus of rigidity, κ is Kolosov's constant, and it is equal to $3-4\nu$ in plane strain, where ν is Poisson's ratio. The stress kernels $S_{lkh}(r_i,\theta_i,r_j,\theta_j)$ can be derived from the Airy stress functions for a dislocation near a circular hole. Theses kernels are given explicitly in [3] as shown in appendix A, equations (A.1)-(A.6). These stress kernel have three subscripts, the first subscript indicates the component of the dislocation Burgers vector, while the two other subscripts indicate the component of stress produced in the field point.

In a polar coordinate system, the stress state induced in an infinite plate containing a circular hole at a field point, i, due to a single dislocation at a source point, j, with strength $|b|_j$ and direction ϕ_j, hence with radial and tangential components $|b|_j\cos\phi_j$ and $|b|_j\sin\phi_j$, respectively (Figure 2.5), as was found by Dundurs and Mura [12], can be written as:

$$\sigma_{rr}^{d} = \frac{\mu}{\pi(\kappa+1)}\left[G_{rrr}\left(r_i,\theta_i,r_j,\theta_j\right)\cos\phi_j + G_{\theta rr}\left(r_i,\theta_i,r_j,\theta_j\right)\sin\phi_j\right]|b|_j \tag{2.8}$$

$$\sigma^d_{\theta\theta} = \frac{\mu}{\pi(\kappa+1)}\left[G_{r\theta\theta}\left(r_i,\theta_i,r_j,\theta_j\right)\cos\phi_j + G_{\theta\theta\theta}\left(r_i,\theta_i,r_j,\theta_j\right)\sin\phi_j\right]|b|_j \tag{2.9}$$

$$\sigma^d_{r\theta} = \frac{\mu}{\pi(\kappa+1)}\left[G_{rr\theta}\left(r_i,\theta_i,r_j,\theta_j\right)\cos\phi_j + G_{\theta r\theta}\left(r_i,\theta_i,r_j,\theta_j\right)\sin\phi_j\right]|b|_j \tag{2.10}$$

By rotating the stress kernels $S_{lkh}(r_i,\theta_i,r_j,\theta_j)$ for the dislocation in all four quadrant to the polar coordinates of the point at position (r_i,θ_i) at which the stress is calculated using the technique of elementary Mohr's circle, the six influence coefficients $G_{lkh}(r_i,\theta_i,r_j,\theta_j)$ can be obtained. They are straight forward but lengthy, and they implicitly take into account the three other dislocations located symmetrically in the three other quadrants. Theses coefficients are given explicitly in [13] as shown in appendix A, equations (A.8)-(A.13). They are calculated and stored for each possible field point, i, with respect to each dislocation insertion point, j.

The components of the accumulated stress $\tilde{\sigma}_{kh}$, at any load step, are calculated as the sum of the stress due to all the dislocations inserted in previous load steps, in addition to the components of the elastic stress. For the first load step at the elastic limit, the stresses $\tilde{\sigma}_{kh}$ are only due to the elastic stress, as no dislocations have been added yet. They are calculated at the beginning of each load step at the grid points in the following way:

$$\tilde{\sigma}_{rr} = \sigma^{elastic}_{rr} + \sigma^d_{rr} \tag{2.11}$$

$$\tilde{\sigma}_{\theta\theta} = \sigma^{elastic}_{\theta\theta} + \sigma^d_{\theta\theta} \tag{2.12}$$

$$\tilde{\sigma}_{r\theta} = \sigma^{elastic}_{r\theta} + \sigma^d_{r\theta} \tag{2.13}$$

As the plastic flow direction is related to the instantaneous local stress state

through the chosen flow rule, the problem is an incremental one. By increasing the applied load, the elastic limit is attained when the yield criterion is first exceeded. This yielding happens at two points on the surface of the hole, on the axis perpendicular to the direction of loading. Under plane strain conditions, the yield condition can be written as a function of the yield strength of the material in shear, k, and the maximum shear stress τ_{max}. The yield strength in shear, k, is equal to $\sigma_Y/2$ in Tresca's yield criterion, and $\sigma_Y/\sqrt{3}$ in von Mises yield criterion, where σ_Y is the yield stress of the material in tension. Therefore, anywhere in the material, the yield condition is exceeded if:

$$\tau_{max} > k \tag{2.14}$$

For a Tresca material, the yield criterion is exact, while for a von Mises material, it is an approximation if $\nu \neq 0.5$, where a deviation in the in-plane slip direction occurs due to yielding caused by the out of plane principal stress, $\sigma_2 = \nu(\sigma_1 - \sigma_3)$. This deviation is small for a material with $\nu = 0.3$ and accurate results can be obtained through equation (2.14).

The yield condition in equation (2.14) can be rewritten in terms of the accumulated stress calculated in the instantaneous maximum shear stress direction as follows:

$$\tilde{\sigma}_{\acute{x}\acute{y}}^{\phi_i} > k \tag{2.15}$$

Where the local coordinate set $(\acute{x}, \acute{y})$ is rotated anticlockwise through an angle $(\theta_i + \phi_i)$ from the global X-axis and oriented in the instantaneous maximum shear stress direction. The components of the accumulated stress in equations (2.11)-

(2.13) are computed at the grid points in order to be used for the calculation of the instantaneous maximum shear stress direction ϕ_i as follows:

$$\phi_i = \frac{1}{2} tan^{-1}\left(\frac{2\tilde{\sigma}_{r\theta}}{\tilde{\sigma}_{rr} - \tilde{\sigma}_{\theta\theta}}\right) + \frac{\pi}{4} \tag{2.16}$$

The accumulated stress in equation (2.15), $\tilde{\sigma}_{\acute{x}\acute{y}}$, at any load increment, is obtained by transforming the accumulated stress components in equations (2.11)-(2.13) through the angle ϕ_i as shown in the following equation.

$$\tilde{\sigma}_{\acute{x}\acute{y}}^{\phi_i} = -\frac{1}{2}(\tilde{\sigma}_{rr} - \tilde{\sigma}_{\theta\theta}) \sin 2\phi_i + \tilde{\sigma}_{r\theta} \cos 2\phi_i \tag{2.17}$$

After reaching the elastic limit, the load is increased by some amount above the elastic limit. This results in a small zone Ω where the yield condition is exceeded. The yield condition in equation (2.15) is now checked at the grid points. The n points where the yield condition is exceeded are called active collocation points. n dislocations are now evenly inserted in the positions between the collocation points to satisfy the yield criterion again. At each active collocation point, the initial maximum shear stress direction is calculated using equation (2.16) in order to obtain n values for ϕ_i. The n values of the initial maximum shear stress directions at the dislocations insertion points ϕ_j are calculated by interpolation from the directions of the four surrounding collocation points ϕ_i.

Now everywhere within that plastic zone Ω,

$$\sigma_{\acute{x}\acute{y}}^{d} + \tilde{\sigma}_{\acute{x}\acute{y}}^{\phi_i} = k \tag{2.18}$$

The total shear stress in the maximum direction is the sum of the accumulated stress $\tilde{\sigma}_{\acute{x}\acute{y}}$ in addition to the current stress state due to the distribution of new set of dislocations, $\sigma^{d}_{\acute{x}\acute{y}}$. As the strength of a single dislocation at point j is $|b|_j$ and its direction is ϕ_j, equation (2.18) can be rewritten, so that for any point within the plastic zone Ω,

$$\begin{aligned}&\sum_{j=1}^{n}\left[K^{\phi_i}_{r\acute{x}\acute{y}}(r_i,\theta_i,r_j,\theta_j,\phi_i)\cos\phi_j + K^{\phi_i}_{\theta\acute{x}\acute{y}}(r_i,\theta_i,r_j,\theta_j,\phi_i)\sin\phi_j\right]|b|_j \\ &= k - \tilde{\sigma}^{\phi_i}_{\acute{x}\acute{y}} \qquad for\ i = 1,n\end{aligned} \tag{2.19}$$

Where the influence functions $K^{\phi_i}_{r\acute{x}\acute{y}}(r_i,\theta_i,r_j,\theta_j,\phi_i)$ and $K^{\phi_i}_{\theta\acute{x}\acute{y}}(r_i,\theta_i,r_j,\theta_j,\phi_i)$ are the shear stress at a field point i whose position is (r_i,θ_i) in the local coordinate set $(\acute{x},\acute{y})$, due a unit dislocation in the r- and θ-directions, respectively, at a non-coincident point, j whose position is (r_j,θ_j). These functions are obtained by transforming the kernels from equations (2.8)-(2.10) through an angle ϕ_i and include the three image dislocations in the other three quadrants. They give the shear stress in the local coordinate set $(\acute{x},\acute{y})$ by being multiplied by the component of the dislocation strength. They are listed in the following equations.

$$\begin{aligned}K^{\phi_i}_{r\acute{x}\acute{y}}(r_i,\theta_i,r_j,\theta_j,\phi_i) &= \frac{\mu}{\pi(\kappa+1)}\{-\frac{1}{2}[G_{rrr}(r_i,\theta_i,r_j,\theta_j) - G_{r\theta\theta}(r_i,\theta_i,r_j,\theta_j)]\sin 2\phi_i \\ &+ G_{rr\theta}(r_i,\theta_i,r_j,\theta_j)\cos 2\phi_i\}\end{aligned} \tag{2.20}$$

$$K^{\phi_i}_{\theta\acute{x}\acute{y}}(r_i,\theta_i,r_j,\theta_j,\phi_i) = \frac{\mu}{\pi(\kappa+1)}\{-\frac{1}{2}[G_{\theta rr}(r_i,\theta_i,r_j,\theta_j) - G_{\theta\theta\theta}(r_i,\theta_i,r_j,\theta_j)]\sin 2\phi_i + G_{\theta r\theta}(r_i,\theta_i,r_j,\theta_j)\cos 2\phi_i\} \tag{2.21}$$

By satisfying equation (2.19) at each active collocation point, i, a set of n simultaneous solvable equations in the n unknown dislocation strengths, $|b|_j$, can be obtained, for given Burgers vector directions, ϕ_j. The $n \times n$ system of linear equations in equation (2.19) can be solved using a standard LU factorization routine with partial pivoting and iterative refinement. The angle ϕ_j is calculated initially as the maximum shear stress direction at each load increment as mentioned previously, and therefore $|b|_j$ can be calculated initially. The next step in the calculation is to calculate the resultant stress state due to this distribution of dislocations in addition to the current accumulated stress. If the yield criterion is checked again, it will be observed that it is exceeded over a new larger region Ω due to the redistribution of stresses. The flow condition can only be satisfied if the local $\acute{x}$ axis, which is aligned with the angle ϕ_i, is in the direction of the maximum shear stress. Therefore, an iterative process is a must in order to improve the solution and to satisfy the normality condition and the flow rule.

The six influence coefficients $G_{lkh}(r_i,\theta_i,r_j,\theta_j)$ related to each dislocation position are calculated and stored, in order to calculate the kernels for equation (2.19), and also to calculate the resultant stress state as follows:

$$\sigma_{rr} = \tilde{\sigma}_{rr} + \frac{\mu}{\pi(\kappa+1)}\sum_{j=1}^{n}\Big[G_{rrr}(r_i,\theta_i,r_j,\theta_j)\cos\phi_j + G_{\theta rr}(r_i,\theta_i,r_j,\theta_j)\sin\phi_j\Big]|b|_j \tag{2.22}$$

$$\sigma_{\theta\theta} = \tilde{\sigma}_{\theta\theta} + \frac{\mu}{\pi(\kappa+1)} \sum_{j=1}^{n} \Big[G_{r\theta\theta}(r_i, \theta_i, r_j, \theta_j) \cos\phi_j + G_{\theta\theta\theta}(r_i, \theta_i, r_j, \theta_j) \sin\phi_j \Big] |b|_j \tag{2.23}$$

$$\sigma_{r\theta} = \tilde{\sigma}_{r\theta} + \frac{\mu}{\pi(\kappa+1)} \sum_{j=1}^{n} \Big[G_{rr\theta}(r_i, \theta_i, r_j, \theta_j) \cos\phi_j + G_{\theta r\theta}(r_i, \theta_i, r_j, \theta_j) \sin\phi_j \Big] |b|_j \tag{2.24}$$

We need to ensure that the maximum shear stress arises on the plane where the plastic flow occurs, as the increment of plastic flow happens in the direction of the dislocation Burgers vector ϕ_j. The problem is only satisfied exactly when ϕ_j is the maximum shear stress direction, which is not known a priori. Hence we will use an iterative solution technique. The angle ϕ_i is initially approximated using the values of the accumulated stress from the previous load step using equation (2.16). The components of the resultant stress state are computed after each iteration using equations (2.22)-(2.24) in order to calculate the new maximum shear stress direction using the following expression:

$$\phi_i = \frac{1}{2} \tan^{-1}\left(\frac{2\sigma_{r\theta}}{\sigma_{rr} - \sigma_{\theta\theta}} \right) + \frac{\pi}{4} \tag{2.25}$$

Convergence of the iterative process occurs when the direction of the maximum shear stress calculated at the end of the load step is equal to the initially calculated flow direction that was used to calculate the strengths of the distributed dislocations.

Chapter 3

Numerical implementation

MATLAB has been used for the numerical modelling of plasticity of an infinite plate containing a circular hole under remote tension, and under plane strain conditions. The material studied here is structural steel with modulus of rigidity $\mu = 77\ GPa$, young's modulus $E = 200\ GPa$, Poisson's ratio $\nu = 0.3$ and yield strength in tension $\sigma_Y = 0.25\ GPa$. This material has an elastic-perfectly plastic stress strain curve with no work hardening. Because of symmetry, only the first quadrant is considered in modelling the plasticity. Yielding first occurs at two points on the surface of the hole, on the axis perpendicular to the direction of loading, that is, at a point with position $(r = 1, \theta = 0)$. At the elastic limit, the elastic stress component $\sigma_{\theta\theta}$ must be equal to the yield strength in tension, hence:

$$\sigma_{\theta\theta}(r = 1, \theta = 0) = \frac{\sigma_0}{2}\left(1 + \frac{1}{1}\right) + \frac{\sigma_0}{2}\left(1 + \frac{3}{1}\right)\cos 0 = 3\sigma_0 \equiv \sigma_Y \tag{3.1}$$

Tresca's yield criterion was employed and the flow direction is the maximum shear stress direction under plane strain conditions. According to Tresca's yield

criterion, $k = \sigma_Y/2$. By substituting for σ_Y in equation (3.1), the elastic limit can be found and it is reached at $\sigma_0/k = 2/3$.

A MATLAB function was set up for the calculation of the six influence coefficients $G_{lkh}(r_i, \theta_i, r_j, \theta_j)$. This MATLAB function was being recalled in another MATLAB function which was set up for the calculation of the polar components of the elastic stresses $\sigma_{kh}^{elastic}$ for use in equations (2.2)-(2.4), the polar components of the stresses due to dislocations σ_{kh}^{d} for use in equations (2.8)-(2.10), and the kernels $K_{r\acute{x}\acute{y}}^{\phi_i}(r_i, \theta_i, r_j, \theta_j, \phi_i)$ and $K_{\theta\acute{x}\acute{y}}^{\phi_i}(r_i, \theta_i, r_j, \theta_j, \phi_i)$ for use in equation (2.19).

An array of probable dislocation sites was positioned in the vicinity of the expected plastic zone as shown in Figure 2.4. A set of pseudo squares was formed by forming the array from a set of radial lines at $w = 1^\circ$ angular spacing, and a set of circular arcs arranged at rw radial spacing, where r is normalized to the radius of the hole, a, while maintaining an aspect ratio equal to $1:1$ for the array. At the beginning of each load step, the six coefficients $G_{lkh}(r_i, \theta_i, r_j, \theta_j)$ are calculated and stored for each possible field point with respect to each active dislocation insertion point. The polar components of the elastic stress, $\sigma_{kh}^{elastic}$, and the stress due to dislocations from previous load steps, σ_{kh}^{d}, are calculated at each grid point using equations (2.2)-(2.4) and equations (2.8)-(2.10) respectively, which are used for the calculation of the polar components of the accumulated stress from previous load steps, $\tilde{\sigma}_{kh}$, at each grid point using equations (2.11)-(2.13). The calculated stresses $\tilde{\sigma}_{kh}$ are then used for the initial estimate of the instantaneous maximum shear stress directions ϕ_i at each grid point using equation (2.16), for the subsequent calculation of the total accumulated stress from previous load steps, $\tilde{\sigma}_{\acute{x}\acute{y}}^{\phi_i}$, at each grid point aligned with the $(\acute{x}, \acute{y})$ direction using

equation (2.17).

Now, Tresca's yield criteria can be checked at each grid point using equation (2.15). Calculation of the positions of the active collocation points is achieved by specifying the field points where this yield condition is exceeded. Once the positions of the active collocation points are found, they are interpolated to the positions of the active dislocations insertion points. An initial estimate of the instantaneous maximum shear stress directions at the dislocations insertion points ϕ_j are calculated by interpolation from the directions of the four surrounding collocation points ϕ_i.

The following iterative procedure will now be adopted to take into account the redistribution of stresses associated with plastic flow. The equation (2.19) will be constructed for each active collocation point using the initial estimate of the instantaneous maximum shear stress directions at the dislocations insertion points ϕ_j, in order to calculate the strengths of the dislocations Burgers vector (b_j) at each dislocation insertion point. Then, the polar components of the resultant stress state due to the current distribution of dislocations in addition to the current accumulated stress are calculated at the active collocation points using equations (2.22)-(2.24). Finally at the end of the iterative procedure, a final estimate of the instantaneous maximum shear stress directions ϕ_i at each active collocation point is calculated using equation (2.25). As mentioned before, the final estimates of the instantaneous maximum shear stress directions at the dislocations insertion points ϕ_j are calculated by interpolation from the directions of the four surrounding collocation points ϕ_i. At the end of each iteration, the error between the initial and final estimates of the instantaneous maximum shear

stress directions at the dislocations insertion points ϕ_j is calculated. This iterative procedure will be repeated until the error tends to zero.

The maximum applied load achievable without divergence of the iterative solution procedure was found to be 2.2 times the elastic limit. At higher loads, the signs of the dislocations Burgers vector strength $|b|_j$ oscillate as the Burgers vector density function shows a non-conservative behavior. As the mesh is refined, the oscillatory behavior happens at smaller load steps and divergence of the iterative solution procedure occurs.

The plasticity has been studied up to a load of 2.2 times the elastic limit. The load has been applied in increments of 0.1 times the elastic limit. In Figure 3.1, the contour of the yielded zone as calculated by this procedure is shown for each load step up to a load equivalent to 2.2 times the elastic limit. This load is the maximum load that can be calculated using this procedure, because at any higher load, convergence of the method cannot be achieved as yielding happens over a too large zone.

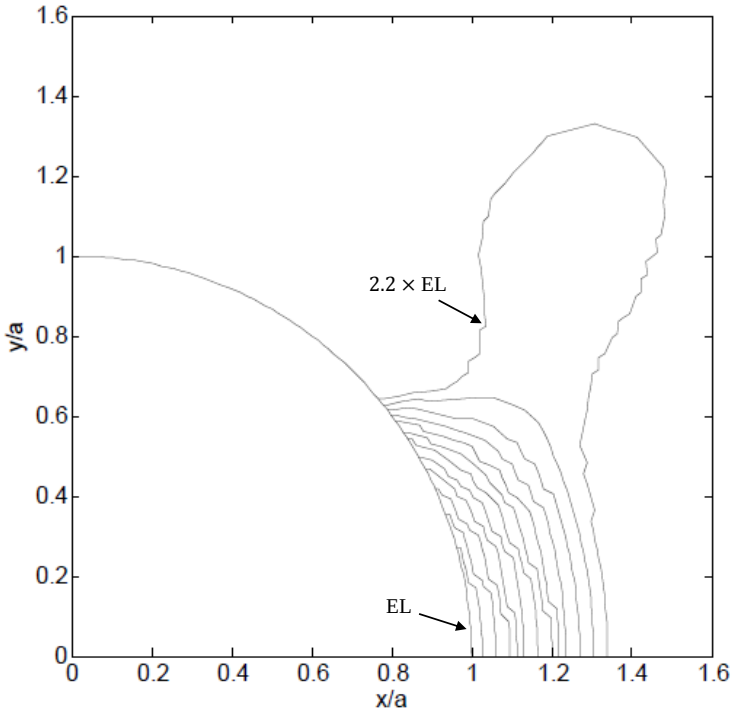

Figure 3.1: Extent of the yielded zone predicted by the distributed dislocations method for each load step up to a load equivalent to 2.2 times the elastic limit in increments of 0.1 times the elastic limit.

Chapter 4

Comparison with FEM calculations

The present problem has been solved numerically using the finite element method. ANSYS Workbench v.15.0 was used for the analysis of a large square plate containing a hole of radius a under remote tension, and under plane strain conditions. The length of each side of the plate studied is equal to $40a$. Only a quarter of the plate is modelled because of symmetry. Tresca's yield criterion is used as a stress tool for the analysis of the yielded zone. Quadrilateral element mesh was used for the meshing. The mesh has been refined around the hole for better modelling of the yielded zone as shown in Figure 4.1. The analysis required only a few minutes to solve the problem.

Tresca's yield contours near the hole are shown in Figure 4.2 for an applied load equal to 2 times the elastic limit. In Figures 4.3-4.15 the extent of the yielded zone is shown for loads up to 2.2 times the elastic limit in increments of 0.1 times the elastic limit, solved using the method implemented here, and using ANSYS Workbench. The locations of the active dislocation insertion points calculated by

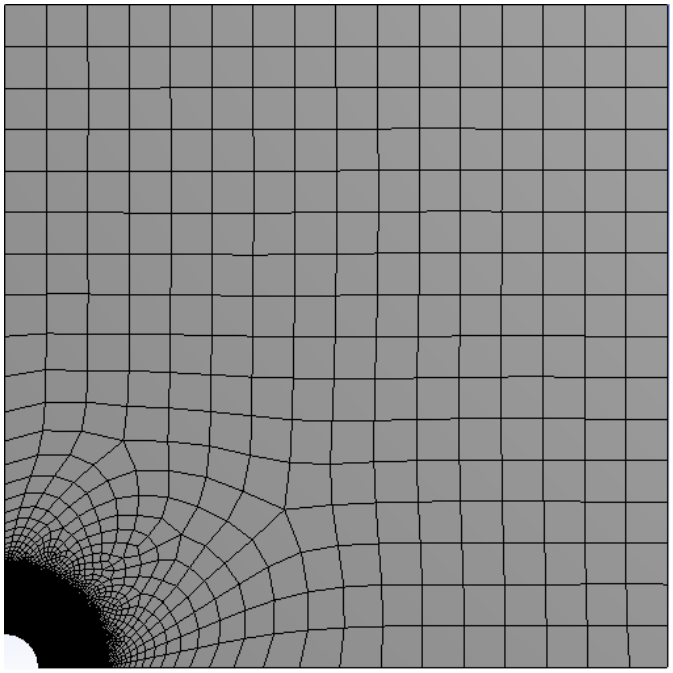

Figure 4.1: FEM meshing of the plate.

the distributed dislocations method are indicated by an ×, while the extent of the yielded zone predicted by the FEM is indicated by the red shaded area. The procedure proposed by Blomerus and Hills applied here shows very good agreement with the FEM results. Their method proved its efficiency to model local plasticity by taking into account the redistribution of stresses that accompanies plastic flow.

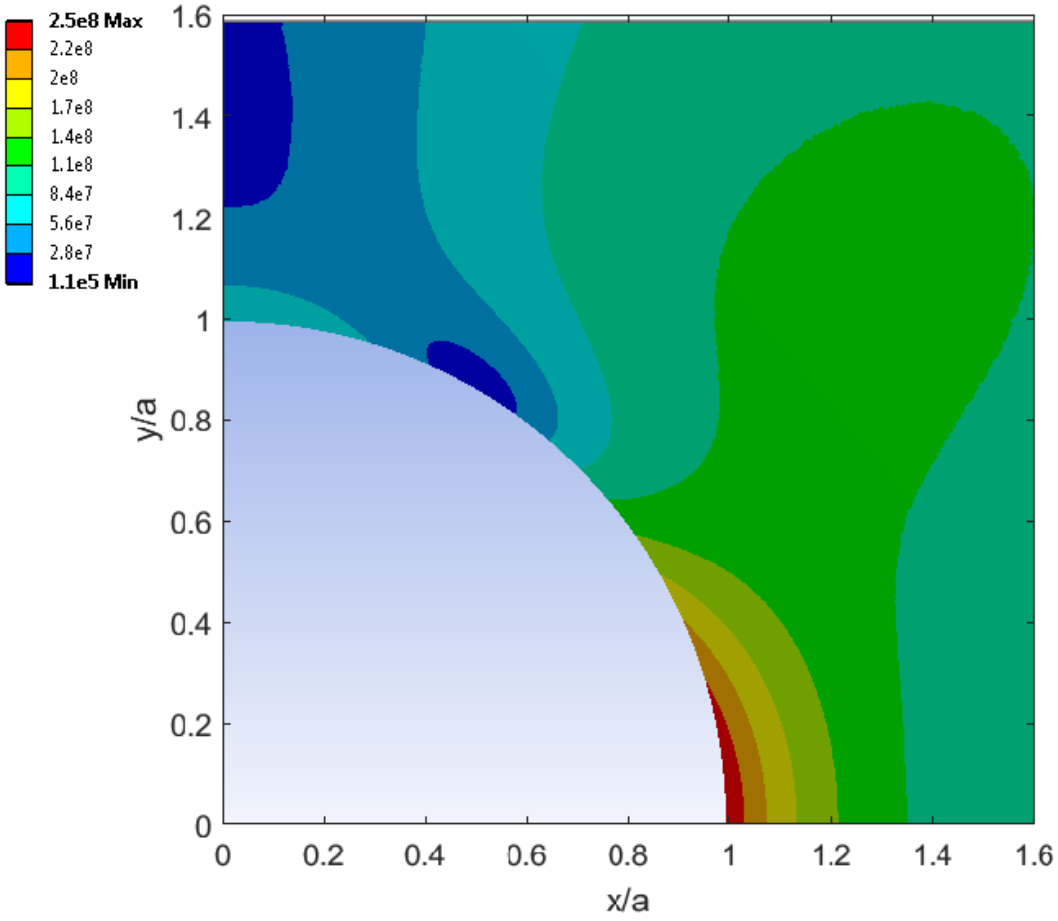

Figure 4.2: Tresca's yield contours around the circular hole.

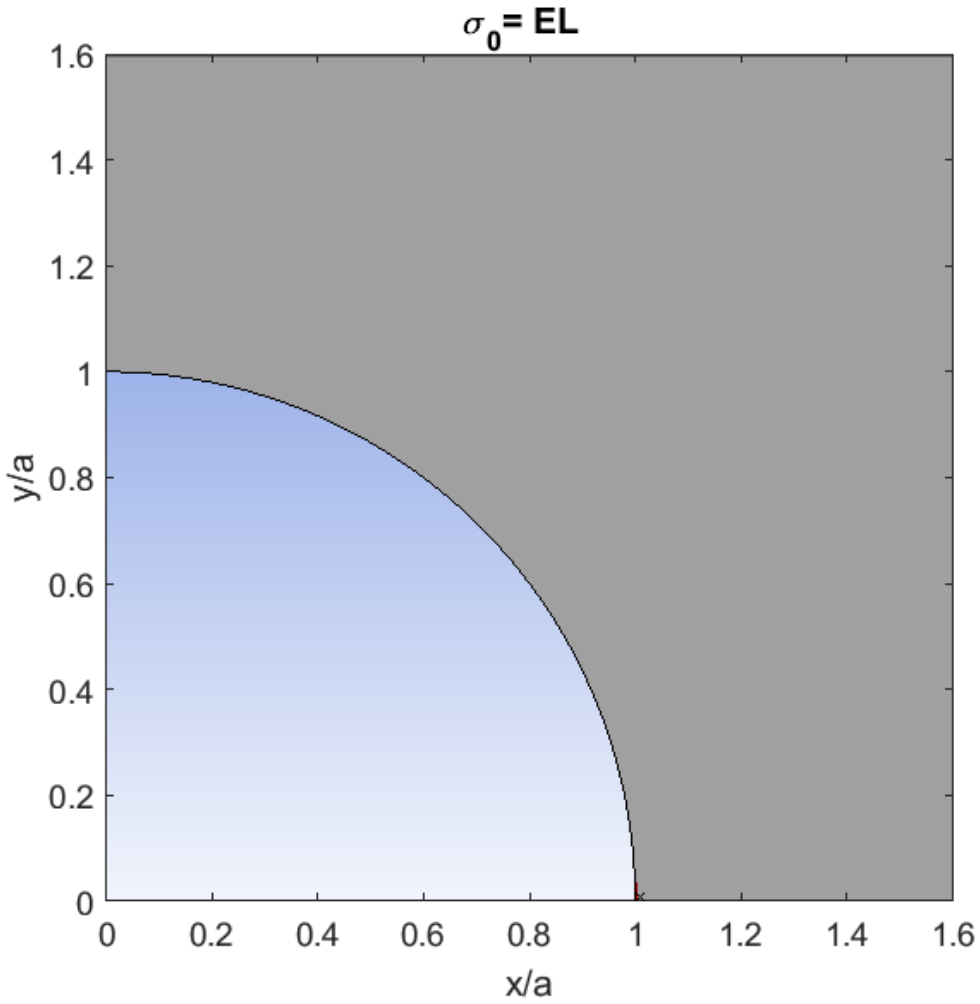

Figure 4.3: Extent of the yielded zone for the FEM method (red area) and the distributed dislocations method (×) for a value of σ_0/EL equivalent to 1.

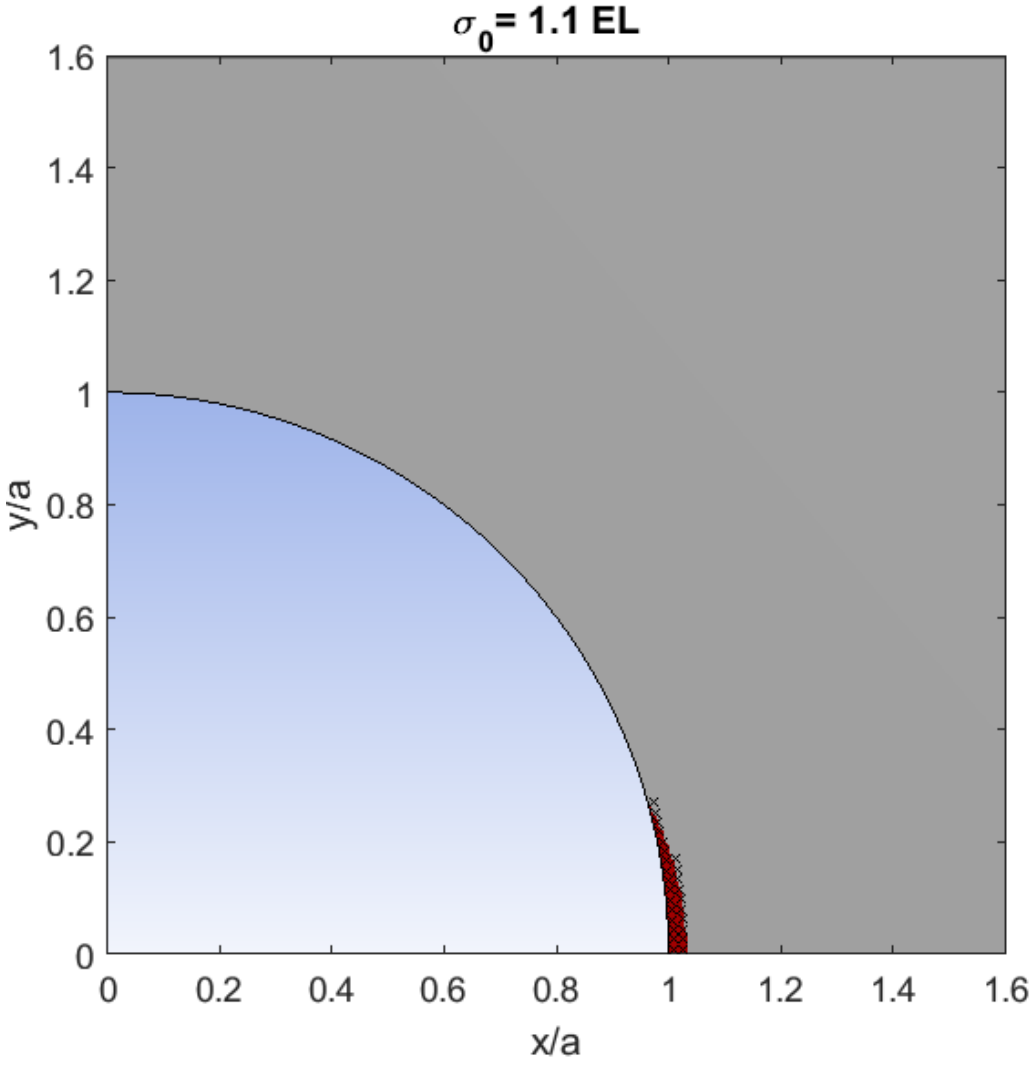

Figure 4.4: Extent of the yielded zone for the FEM method (red area) and the distributed dislocations method (×) for a value of σ_0/EL equivalent to 1.1.

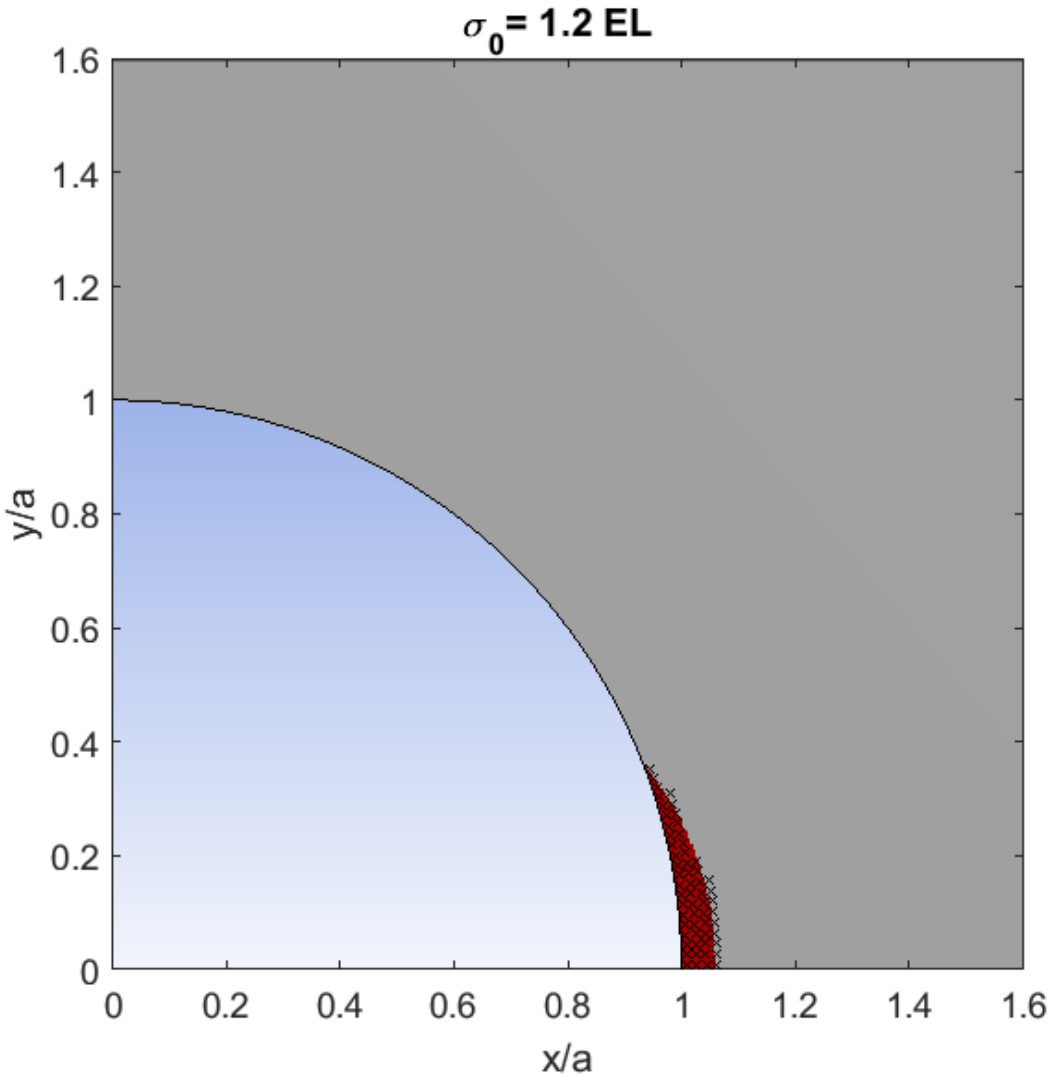

Figure 4.5: Extent of the yielded zone for the FEM method (red area) and the distributed dislocations method (×) for a value of σ_0/EL equivalent to 1.2.

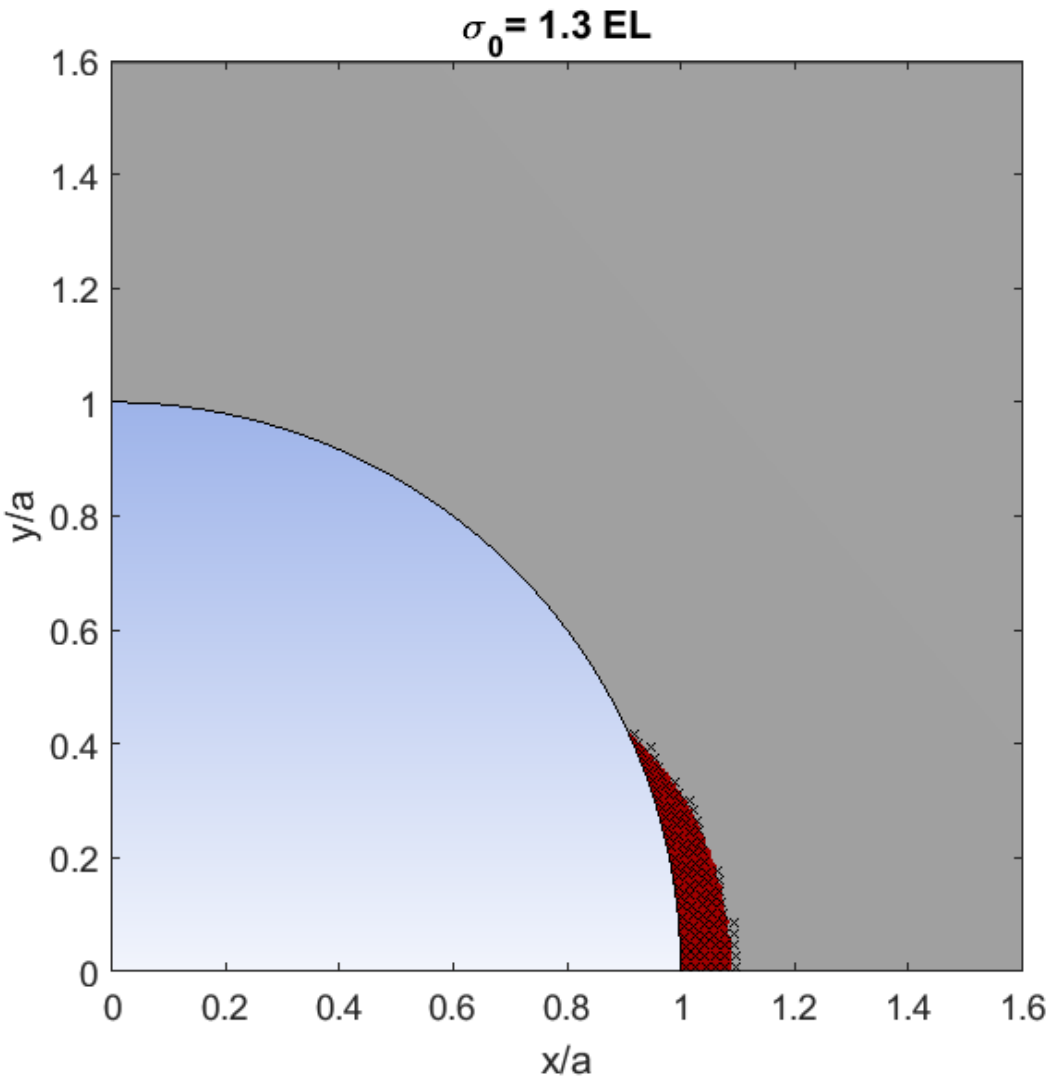

Figure 4.6: Extent of the yielded zone for the FEM method (red area) and the distributed dislocations method (×) for a value of σ_0/EL equivalent to 1.3.

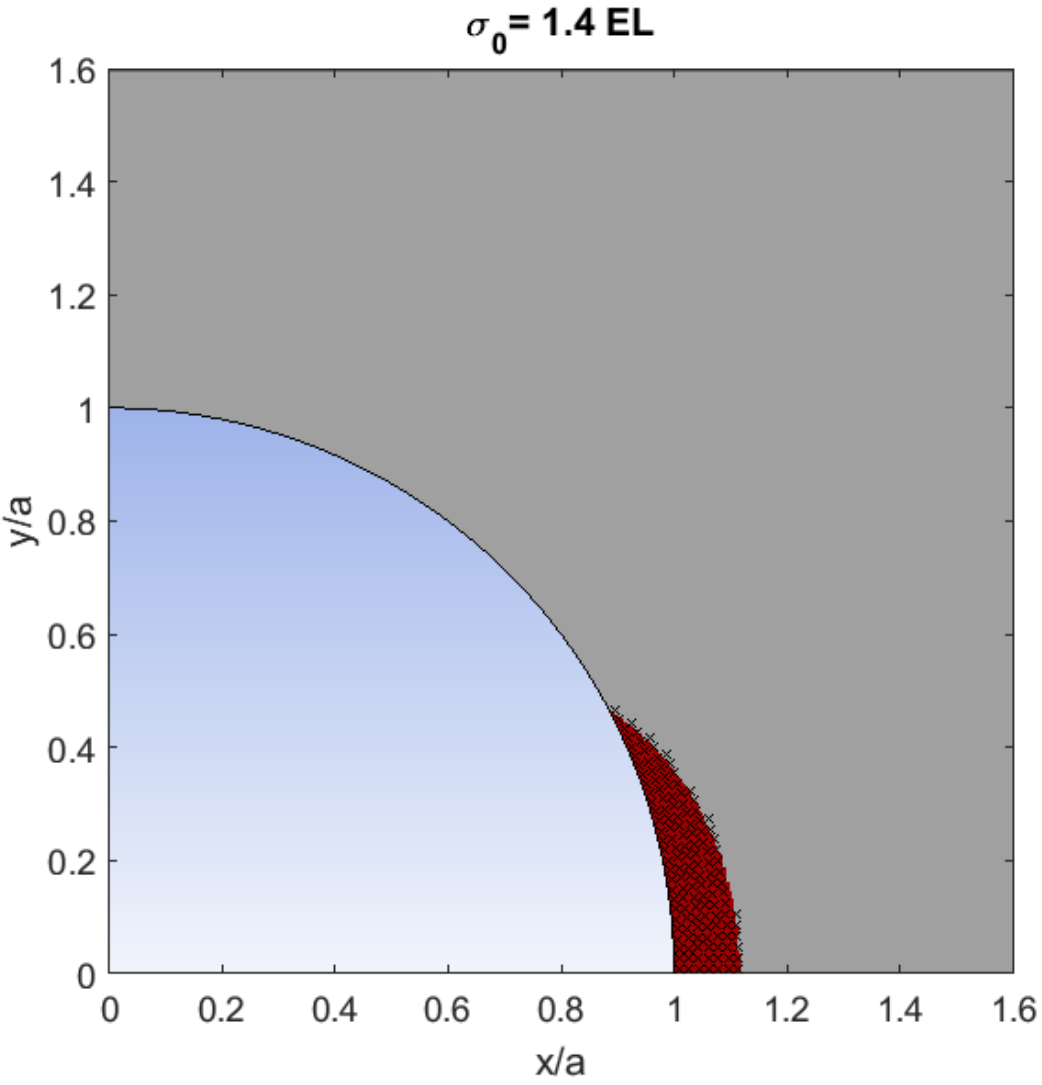

Figure 4.7: Extent of the yielded zone for the FEM method (red area) and the distributed dislocations method (×) for a value of σ_0/EL equivalent to 1.4.

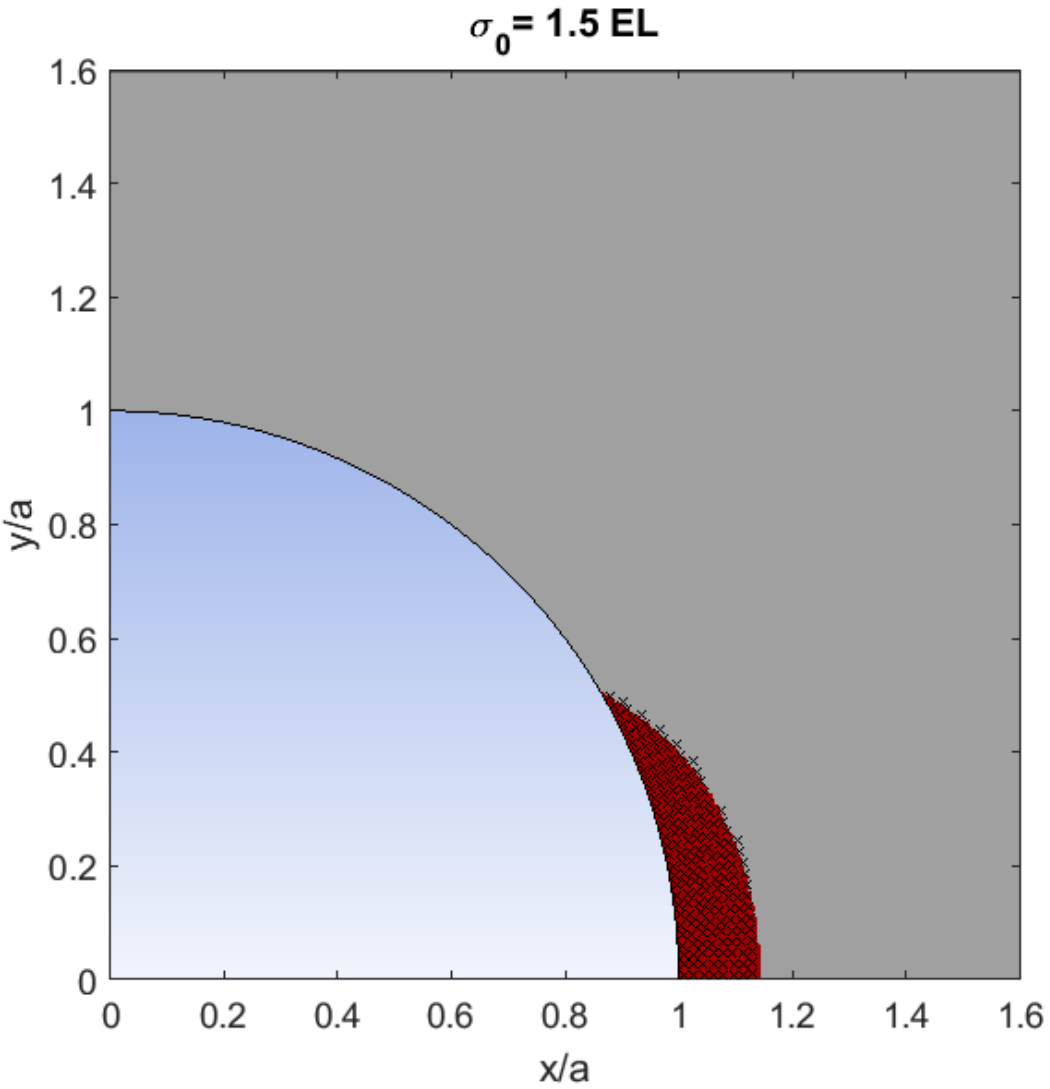

Figure 4.8: Extent of the yielded zone for the FEM method (red area) and the distributed dislocations method (×) for a value of σ_0/EL equivalent to 1.5.

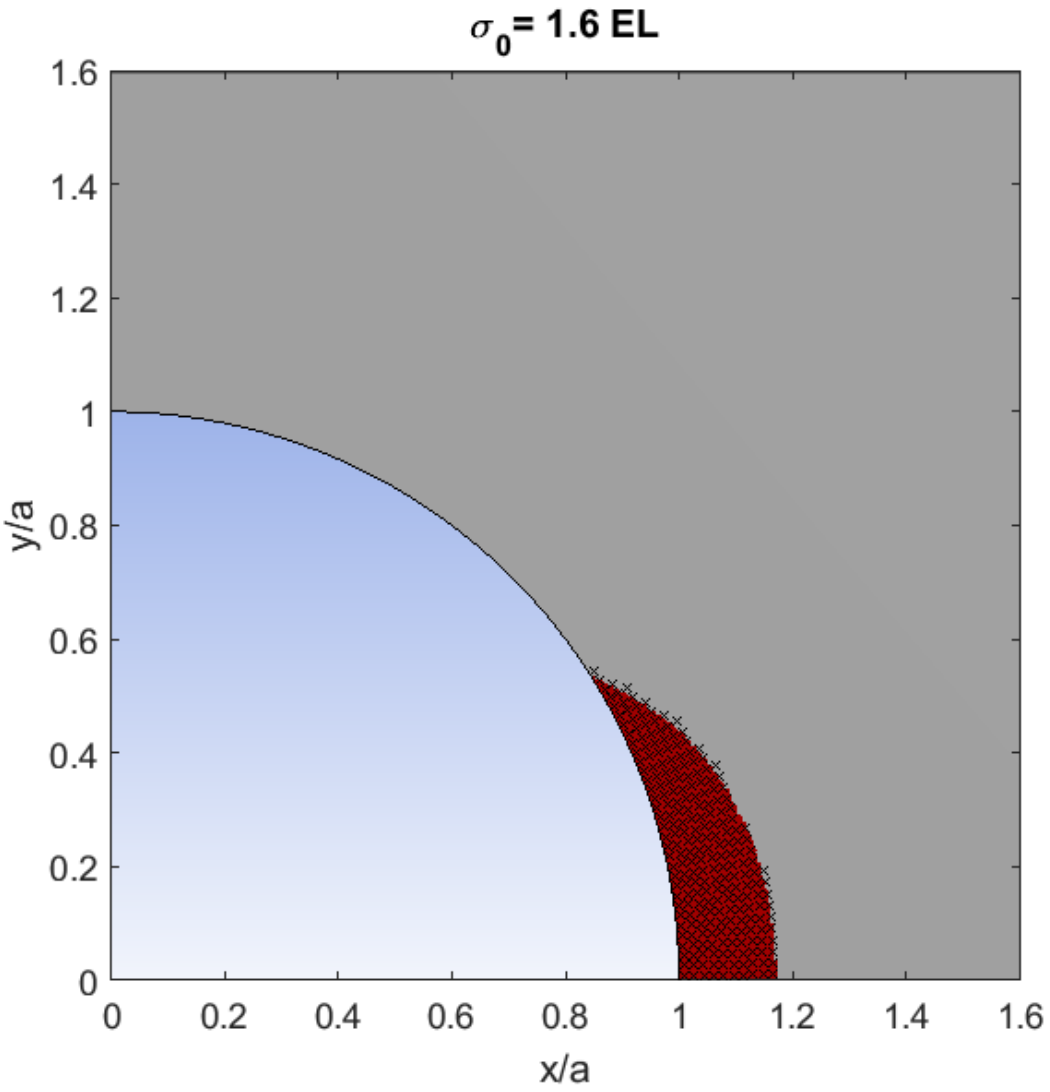

Figure 4.9: Extent of the yielded zone for the FEM method (red area) and the distributed dislocations method (×) for a value of σ_0/EL equivalent to 1.6.

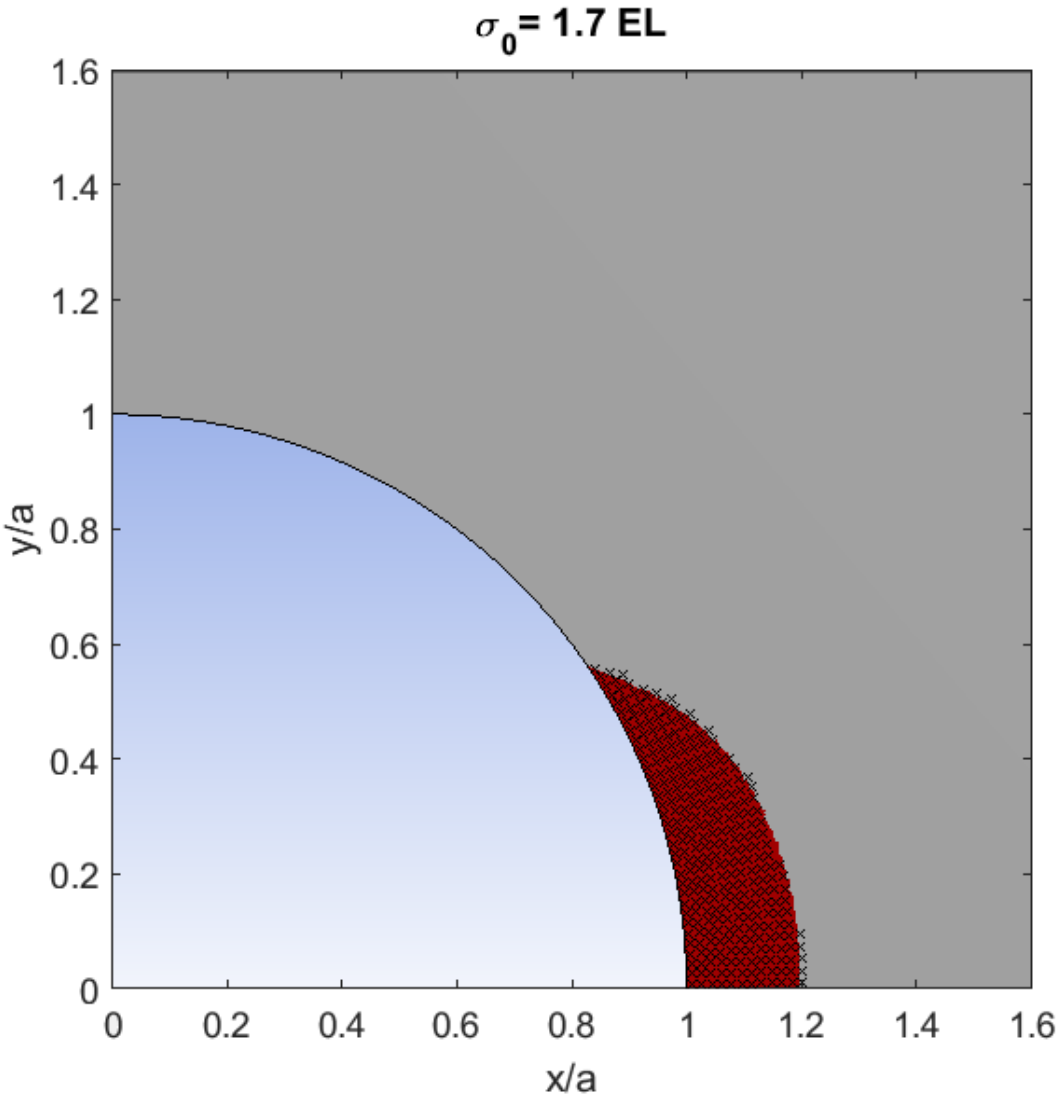

Figure 4.10: Extent of the yielded zone for the FEM method (red area) and the distributed dislocations method (×) for a value of σ_0/EL equivalent to 1.7.

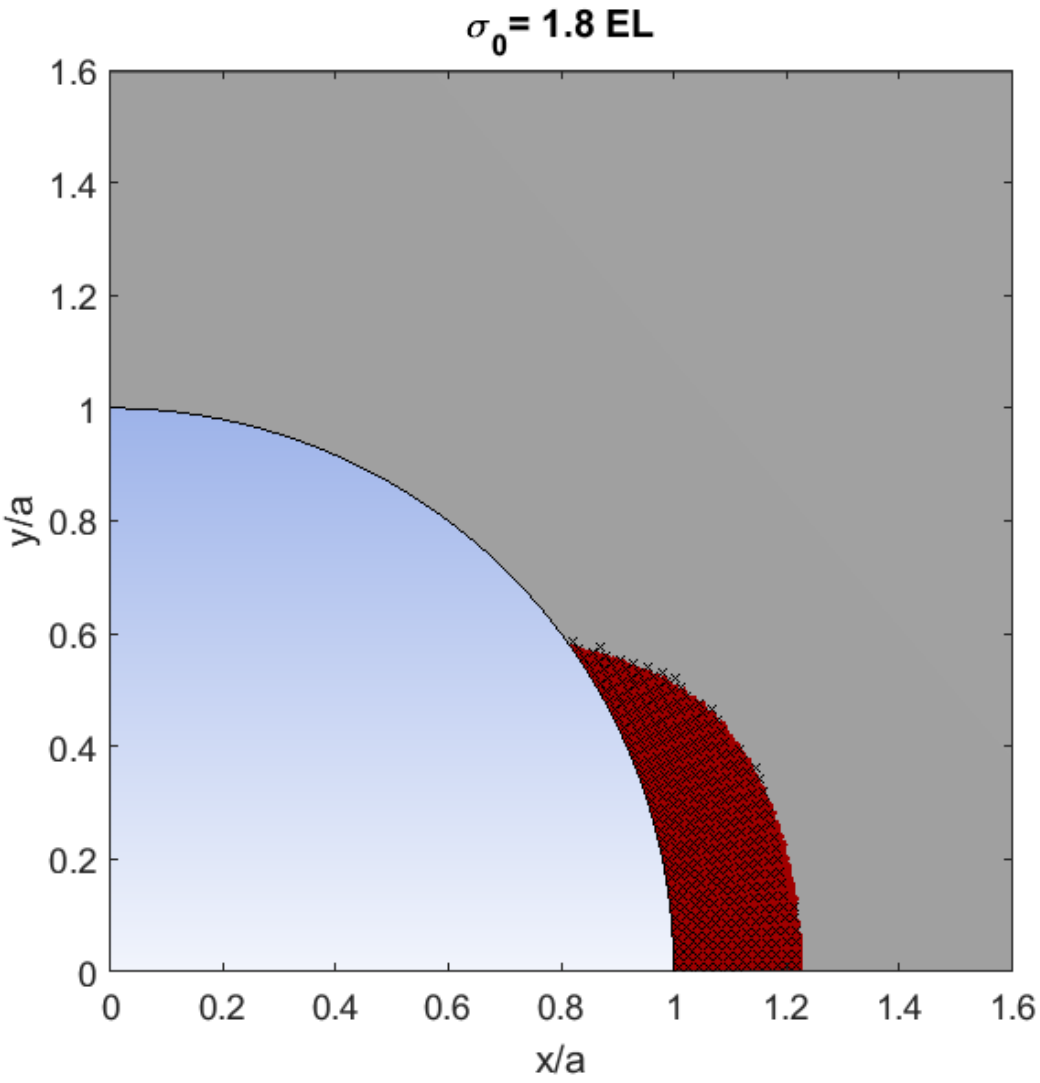

Figure 4.11: Extent of the yielded zone for the FEM method (red area) and the distributed dislocations method (×) for a value of σ_0/EL equivalent to 1.8.

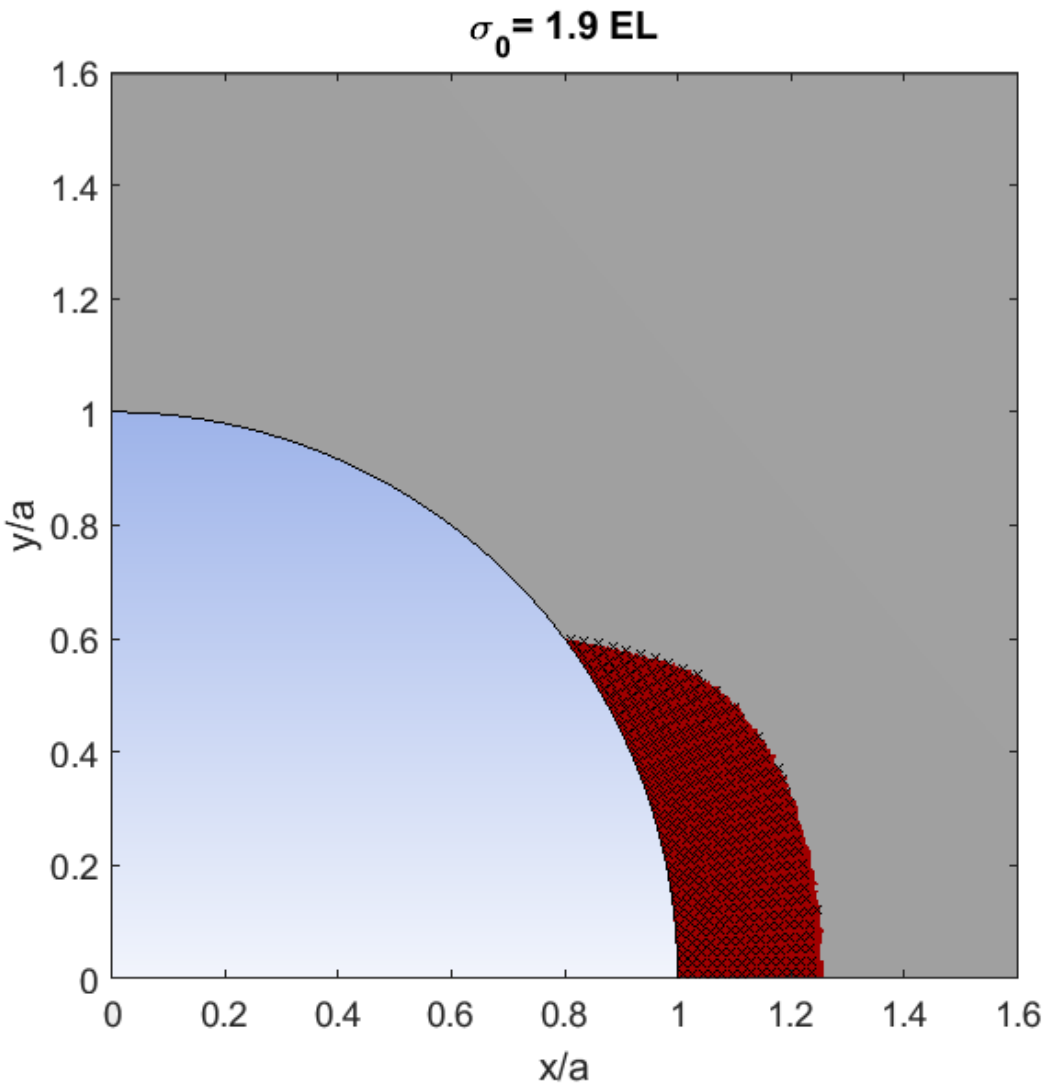

Figure 4.12: Extent of the yielded zone for the FEM method (red area) and the distributed dislocations method (×) for a value of σ_0/EL equivalent to 1.9.

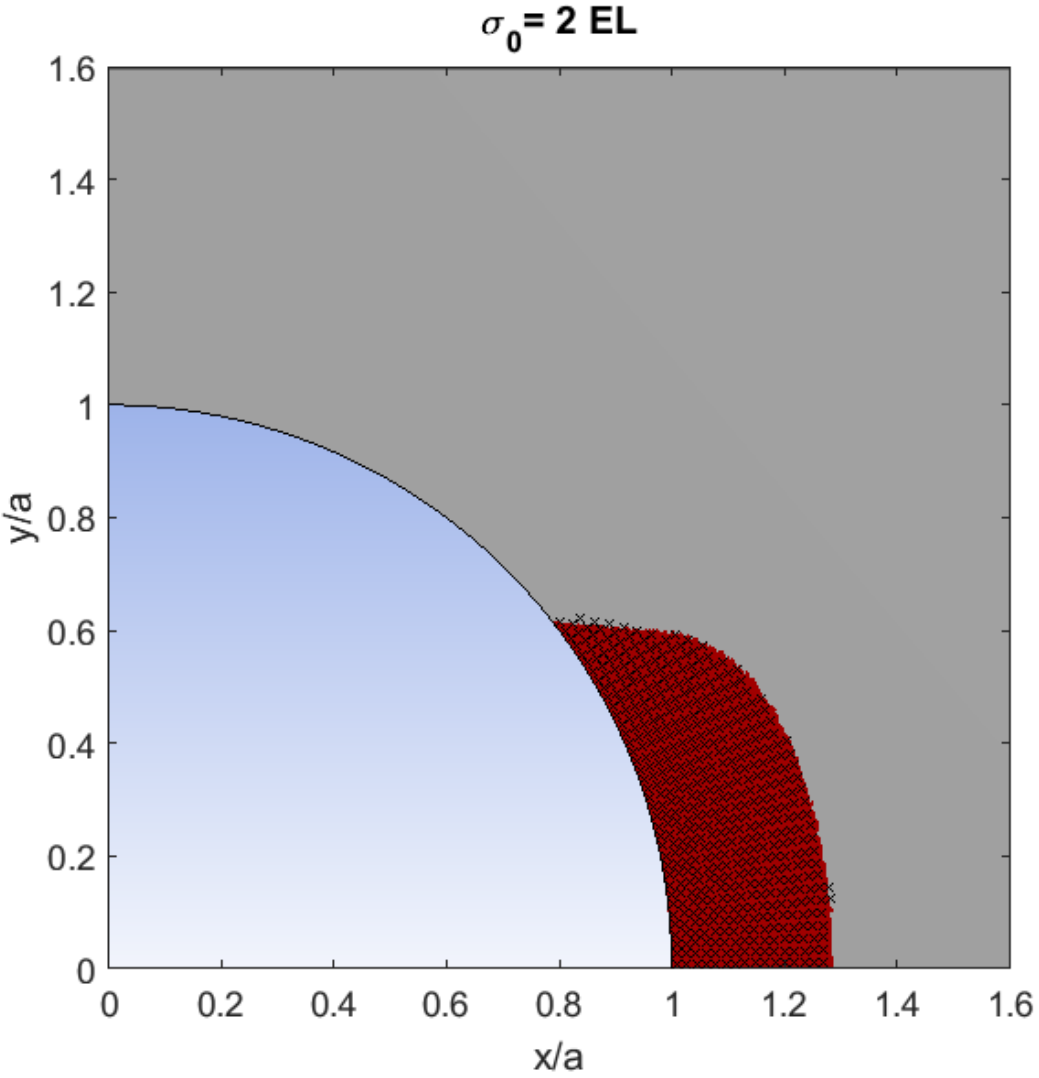

Figure 4.13: Extent of the yielded zone for the FEM method (red area) and the distributed dislocations method (×) for a value of σ_0/EL equivalent to 2.

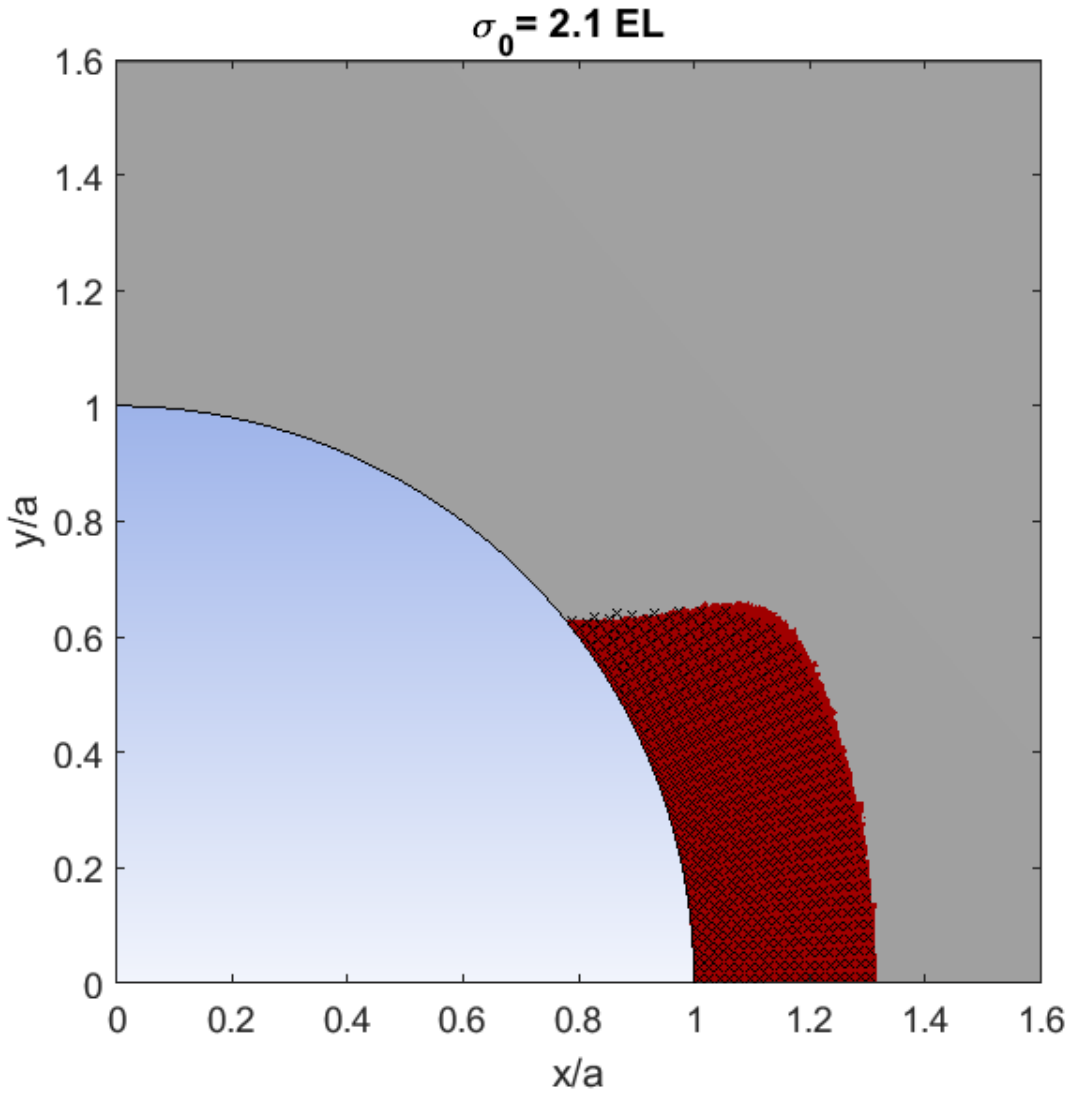

Figure 4.14: Extent of the yielded zone for the FEM method (red area) and the distributed dislocations method (×) for a value of σ_0/EL equivalent to 2.1.

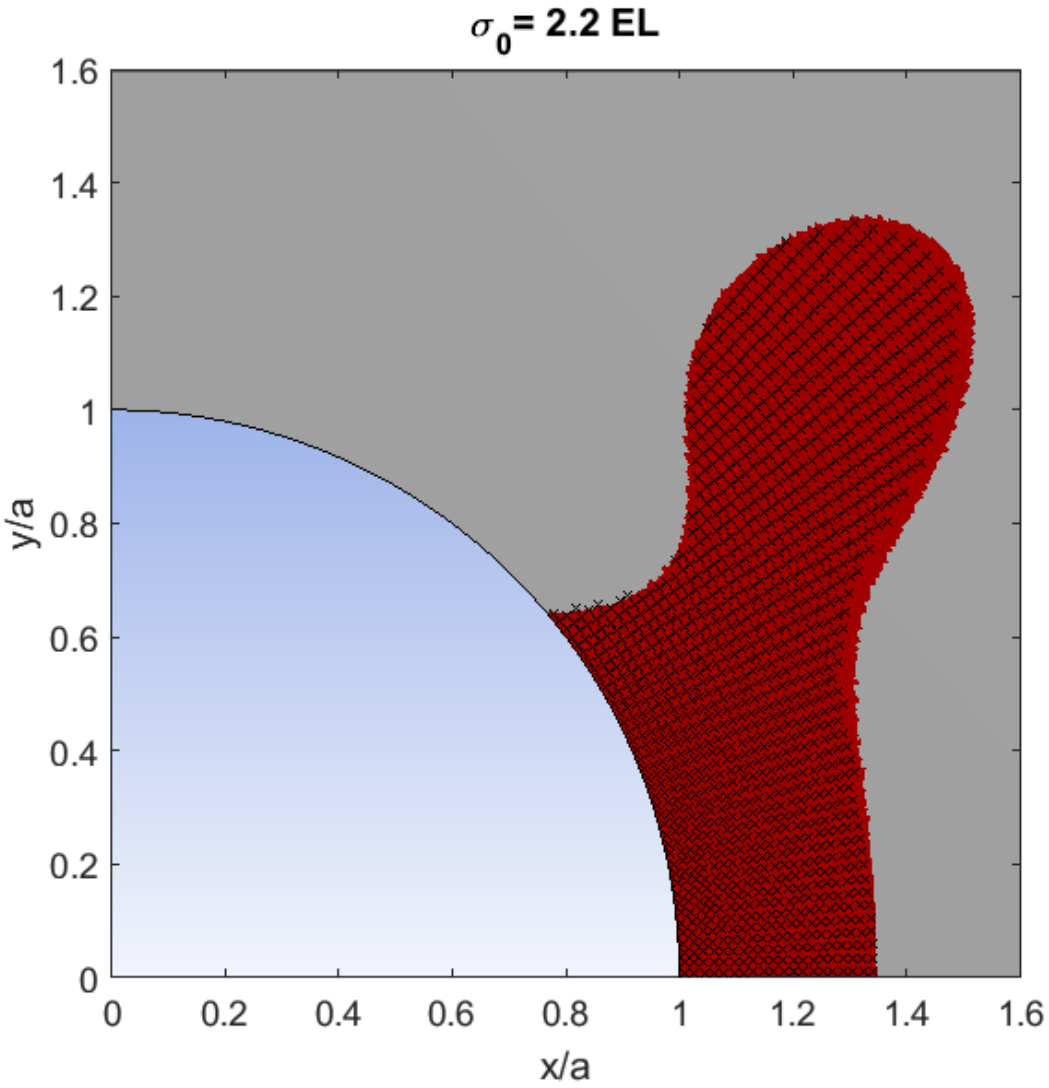

Figure 4.15: Extent of the yielded zone for the FEM method (red area) and the distributed dislocations method (×) for a value of σ_0/EL equivalent to 2.2.

Chapter 5

Conclusion

In this thesis, a procedure proposed by Blomerus and Hills [3] for modelling local plasticity at stress raising features using the distributed dislocations method has been applied for the analysis of an infinite plate containing a circular hole and subject to remote tension under plane strain conditions. This method employs an underlying elasticity solution that takes into account the hole itself. Stationary edge dislocations have been used in order to model yielding at the neighbourhood of the hole where the yield criteria has been exceeded. An iterative technique is adopted in order to align the dislocations Burgers vector with the instantaneous maximum shear stress direction for the flow rule to be met. Their method proved its efficiency to model local plasticity by taking into account the redistribution of stresses in the material that accompanies plastic flow. Their method has shown very good agreement in modeling the local yielding with the results from the finite element analysis. Hence it has proved to combine the advantage of the accuracy of the finite element method as well as the speed of the method of Neu-

ber/Glinka.

Chapter 6

Future work

The present work can be continued in different aspects. On the experimental side, we plan to test a number of specimens of different materials and sizes to actually try to measure the extent of the plastic zones produced. This needs previous characterization of the materials under testing and we need to find out how to ascertain which regions have actually yielded.

On the numerical side, we plan to undertake the formulation for the same geometry but with different loadings such as pure torsion or biaxial combinations of tension and torsion, both applied in-phase and out-of-phase. It may happen that the agreement between the results of the dislocations' formulation and the FEM solutions is not as good for these loading as it is for pure and simple tension. The results are expected to be fine for the in-phase loadings. The out-of-phase loading case seems quite intriguing.

Finally, it would be interesting to make the formulation for other geometries. Elliptical notches and V-notches would be very interesting. Of course, the dif-

ficulty here resides in that we do not have the ”fundamental” solution of the dislocation field in the presence of notches of such geometries, we do not have the Dundurs and Mura solution. The elliptical case may be achievable from the circular case using conformal mapping techniques. The V-notch would certainly be more difficult. It might be possible to derive numerical solutions and employ them in the further numerical formulations needed for the plastic zone determination.

Appendices

Appendix A

Stress due to a dislocation near a circular hole

The six stress kernels $S_{lkh}(r_i, \theta_i, r_j, \theta_j)$ can be derived from the Airy stress functions for a dislocation near a circular hole and listed below:

$$S_{xxy} = -\frac{2x_1}{r_1^2} + \frac{4x_1^3}{r_1^4} + \frac{2x_2}{r_2^2} - \frac{4x_2^3}{r_2^4} - \frac{2x}{r_i^2} + \frac{4x^3}{r_i^4} + \frac{6x}{r_i^4} - \frac{8x^3}{r_i^6} - \frac{\left(r_j^2 - 1\right)}{r_j^3} \times \left[\frac{2}{r_2^2} - \frac{16x_2^2}{r_2^4} + \frac{16x_2^4}{r_2^6} - \left(r_j - \frac{1}{r_j}\right)\left(\frac{8x_2^3}{r_2^6} - \frac{6x_2}{r_2^4}\right)\right], \tag{A.1}$$

$$S_{yxy} = -\frac{2y}{r_1^2} + \frac{4x_1^2 y}{r_1^4} + \frac{2y}{r_2^2} - \frac{4x_2^2 y}{r_2^4} - \frac{2y}{r_i^2} + \frac{4x^2 y}{r_i^4} + \frac{2y}{r_i^4} - \frac{8x^2 y}{r_i^6} + \frac{\left(r_j^2 - 1\right)}{r_j^3} \times \left[\frac{4r_j^2 x_2 y}{r_2^4} - \frac{2x_2 y}{r_2^4} + \frac{16x_2^3 y}{r_2^6} - \frac{4r_j^2 xy}{r_i^4} + \left(r_j - \frac{1}{r_j}\right)\left(\frac{2y}{r_2^4} - \frac{8x_2^2 y}{r_2^6}\right)\right], \tag{A.2}$$

$$S_{xxx} = -\frac{2y}{r_1^2} + \frac{4x_1^2 y}{r_1^4} + \frac{2y}{r_2^2} + \frac{4x_2^2 y}{r_2^4} - \frac{2y}{r_i^2} - \frac{4x^2 y}{r_i^4} - \frac{2y}{r_i^6} + \frac{8x^2 y}{r_i^6} - \frac{\left(r_j^2 - 1\right)}{r_j^3} \times \left[\frac{4x_2 y}{r_2^4} - \frac{16x_2^3 y}{r_2^6} - \left(r_j - \frac{1}{r_j}\right)\left(\frac{2y}{r_2^4} - \frac{8x_2^2 y}{r_2^6}\right)\right], \tag{A.3}$$

$$S_{yxx} = -\frac{2x_1}{r_1^2} + \frac{4x_1^2}{r_1^4} + \frac{2x_2}{r_2^2} - \frac{4x_2^3}{r_2^4} - \frac{2x}{r_i^2} + \frac{4x^3}{r_i^4} + \frac{6x}{r_i^4} - \frac{8x^3}{r_i^6} + \frac{\left(r_j^2 - 1\right)}{r_j^3} \times \left[-\frac{2r_j^2}{r_2^2} + \frac{4r_j^2 x_2^2}{r_2^4} - \frac{12x_2^2}{r_2^4} + \frac{16x_2^4}{r_2^6} + \frac{2r_j^2}{r_i^2} - \frac{4x^2 r_j^2}{r_i^4} + \left(r_j - \frac{1}{r_j}\right)\left(\frac{6x_2}{r_2^4} - \frac{8x_2^3}{r_2^6}\right)\right], \tag{A.4}$$

$$S_{xyy} = -\frac{2y}{r_1^2} + \frac{4x_1^2 y}{r_1^4} + \frac{2y}{r_2^2} - \frac{4x_2^2 y}{r_2^4} - \frac{2y}{r_i^2} + \frac{4x^2 y}{r_i^4} + \frac{2y}{r_i^4} - \frac{8x^2 y}{r_i^6} - \frac{\left(r_j^2 - 1\right)}{r_j^3} \times \left[-\frac{12x_2 y}{r_2^4} + \frac{16x_2^3 y}{r_2^6} - \left(r_j - \frac{1}{r_j}\right)\left(-\frac{2y}{r_2^4} + \frac{8x_2^2 y}{r_2^6}\right)\right], \tag{A.5}$$

$$S_{yyy} = \frac{6x_1}{r_1^2} - \frac{4x_1^3}{r_1^4} - \frac{6x_2}{r_2^2} + \frac{4x_2^3}{r_2^4} + \frac{6x}{r_i^2} - \frac{4x^3}{r_i^4} - \frac{6x}{r_i^4} + \frac{8x^3}{r_i^6} + \frac{\left(r_j^2 - 1\right)}{r_j^3} \times \left[\frac{2r_j^2}{r_2^2} - \frac{4r_j^2 x_2^2}{r_2^4} - \frac{4}{r_2^2} + \frac{20x_2^2}{r_2^4} - \frac{16x_2^4}{r_2^6} - \frac{2r_j^2}{r_i^2} - \frac{4x^2 r_j^2}{r_i^4} + \left(r_j - \frac{1}{r_j}\right)\left(-\frac{6x_2}{r_2^4} + \frac{8x_2^3}{r_2^6}\right)\right] \tag{A.6}$$

Where, referring to Figure A.1:

$$\begin{aligned} x &= r\cos\theta \\ y &= r\sin\theta \\ x_1 &= x - r_j \\ x_2 &= x - \frac{1}{r_j} \\ r_1 &= \sqrt{x_1^2 + y^2} \\ r_2 &= \sqrt{x_2^2 + y^2} \end{aligned} \tag{A.7}$$

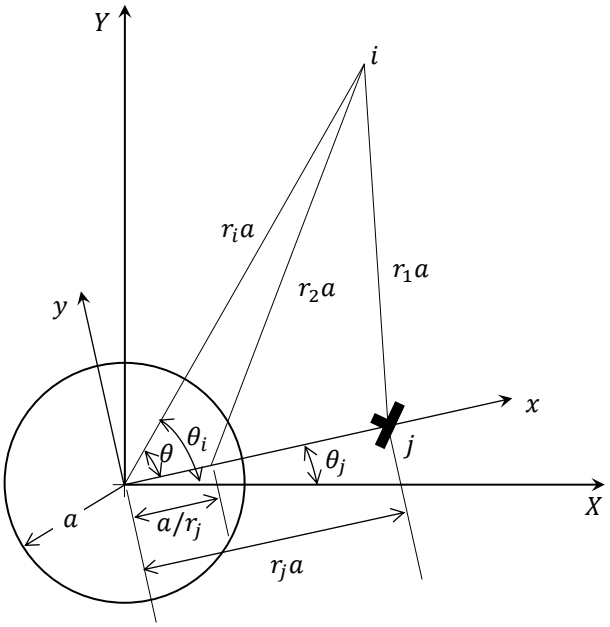

Figure A.1: A dislocation near a circular hole.

The six influence coefficients $G_{lkh}(r_i, \theta_i, r_j, \theta_j)$ are listed below:

$$
\begin{aligned}
G_{rrr} = {} & \{\frac{1}{2}[S_{xxx}(r_i,\theta,r_j) + S_{xyy}(r_i,\theta,r_j)] + \frac{1}{2}[S_{xxx}(r_i,\theta,r_j) - S_{xyy}(r_i,\theta,r_j)]\cos 2\theta \\
& + S_{xxy}(r_i,\theta,r_j)\sin 2\theta\} - \{\frac{1}{2}[S_{xxx}(r_i,\theta_i+\theta_j,r_j) + S_{xyy}(r_i,\theta_i+\theta_j,r_j)] \\
& + \frac{1}{2}[S_{xxx}(r_i,\theta_i+\theta_j,r_j) - S_{xyy}(r_i,\theta_i+\theta_j,r_j)]\cos 2(\theta_i+\theta_j) \\
& + S_{xxy}(r_i,\theta_i+\theta_j,r_j)\sin 2(\theta_i+\theta_j)\} + \{\frac{1}{2}[S_{xxx}(r_i,\pi+\theta,r_j) + S_{xyy}(r_i,\pi+\theta,r_j)] \\
& + \frac{1}{2}[S_{xxx}(r_i,\pi+\theta,r_j) - S_{xyy}(r_i,\pi+\theta,r_j)]\cos 2(\pi+\theta) + S_{xxy}(r_i,\pi+\theta,r_j)\sin 2(\pi+\theta)\} \\
& - \{\frac{1}{2}[S_{xxx}(r_i,\pi+\theta_i+\theta_j,r_j) + S_{xyy}(r_i,\pi+\theta_i+\theta_j,r_j)] + \frac{1}{2}[S_{xxx}(r_i,\pi+\theta_i+\theta_j,r_j) \\
& - S_{xyy}(r_i,\pi+\theta_i+\theta_j,r_j)]\cos 2(\pi+\theta_i+\theta_j) + S_{xxy}(r_i,\pi+\theta_i+\theta_j,r_j)\sin 2(\pi+\theta_i+\theta_j)\},
\end{aligned}
\tag{A.8}
$$

$$
\begin{aligned}
G_{r\theta\theta} = {} & \{\frac{1}{2}[S_{xxx}(r_i,\theta,r_j)+S_{xyy}(r_i,\theta,r_j)]-\frac{1}{2}[S_{xxx}(r_i,\theta,r_j)-S_{xyy}(r_i,\theta,r_j)]\cos 2\theta \\
& - S_{xxy}(r_i,\theta,r_j)\sin 2\theta\}-\{\frac{1}{2}[S_{xxx}(r_i,\theta_i+\theta_j,r_j)+S_{xyy}(r_i,\theta_i+\theta_j,r_j)] \\
& - \frac{1}{2}[S_{xxx}(r_i,\theta_i+\theta_j,r_j)-S_{xyy}(r_i,\theta_i+\theta_j,r_j)]\cos 2(\theta_i+\theta_j) \\
& - S_{xxy}(r_i,\theta_i+\theta_j,r_j)\sin 2(\theta_i+\theta_j)\}+\{\frac{1}{2}[S_{xxx}(r_i,\pi+\theta,r_j)+S_{xyy}(r_i,\pi+\theta,r_j)] \\
& - \frac{1}{2}[S_{xxx}(r_i,\pi+\theta,r_j)-S_{xyy}(r_i,\pi+\theta,r_j)]\cos 2(\pi+\theta)-S_{xxy}(r_i,\pi+\theta,r_j)\sin 2(\pi+\theta)\} \\
& - \{\frac{1}{2}[S_{xxx}(r_i,\pi+\theta_i+\theta_j,r_j)+S_{xyy}(r_i,\pi+\theta_i+\theta_j,r_j)]-\frac{1}{2}[S_{xxx}(r_i,\pi+\theta_i+\theta_j,r_j) \\
& - S_{xyy}(r_i,\pi+\theta_i+\theta_j,r_j)]\cos 2(\pi+\theta_i+\theta_j)-S_{xxy}(r_i,\pi+\theta_i+\theta_j,r_j)\sin 2(\pi+\theta_i+\theta_j)\},
\end{aligned}
\tag{A.9}
$$

$$
\begin{aligned}
G_{rr\theta} = {} & \{-\frac{1}{2}[S_{xxx}(r_i,\theta,r_j)-S_{xyy}(r_i,\theta,r_j)]\sin 2\theta+S_{xxy}(r_i,\theta,r_j)\cos 2\theta\} \\
& - \{-\frac{1}{2}[S_{xxx}(r_i,\theta_i+\theta_j,r_j)-S_{xyy}(r_i,\theta_i+\theta_j,r_j)]\sin 2(\theta_i+\theta_j) \\
& + S_{xxy}(r_i,\theta_i+\theta_j,r_j)\cos 2(\theta_i+\theta_j)\}+\{-\frac{1}{2}[S_{xxx}(r_i,\pi+\theta,r_j) \\
& - S_{xyy}(r_i,\pi+\theta,r_j)]\sin 2(\pi+\theta)+S_{xxy}(r_i,\pi+\theta,r_j)\cos 2(\pi+\theta)\} \\
& - \{-\frac{1}{2}[S_{xxx}(r_i,\pi+\theta_i+\theta_j,r_j)-S_{xyy}(r_i,\pi+\theta_i+\theta_j,r_j)]\sin 2(\pi+\theta_i+\theta_j) \\
& + S_{xxy}(r_i,\pi+\theta_i+\theta_j,r_j)\cos 2(\pi+\theta_i+\theta_j)\},
\end{aligned}
\tag{A.10}
$$

$$
\begin{aligned}
G_{\theta rr} = &\{\frac{1}{2}[S_{yxx}(r_i,\theta,r_j)+S_{yyy}(r_i,\theta,r_j)]+\frac{1}{2}[S_{yxx}(r_i,\theta,r_j)-S_{yyy}(r_i,\theta,r_j)]\cos 2\theta \\
&+S_{yxy}(r_i,\theta,r_j)\sin 2\theta\}+\{\frac{1}{2}[S_{yxx}(r_i,\theta_i+\theta_j,r_j)+S_{yyy}(r_i,\theta_i+\theta_j,r_j)] \\
&+\frac{1}{2}[S_{yxx}(r_i,\theta_i+\theta_j,r_j)-S_{yyy}(r_i,\theta_i+\theta_j,r_j)]\cos 2(\theta_i+\theta_j) \\
&+S_{yxy}(r_i,\theta_i+\theta_j,r_j)\sin 2(\theta_i+\theta_j)\}+\{\frac{1}{2}[S_{yxx}(r_i,\pi+\theta,r_j)+S_{yyy}(r_i,\pi+\theta,r_j)] \\
&+\frac{1}{2}[S_{yxx}(r_i,\pi+\theta,r_j)-S_{yyy}(r_i,\pi+\theta,r_j)]\cos 2(\pi+\theta)+S_{yxy}(r_i,\pi+\theta,r_j)\sin 2(\pi+\theta)\} \\
&+\{\frac{1}{2}[S_{yxx}(r_i,\pi+\theta_i+\theta_j,r_j)+S_{yyy}(r_i,\pi+\theta_i+\theta_j,r_j)]+\frac{1}{2}[S_{yxx}(r_i,\pi+\theta_i+\theta_j,r_j) \\
&-S_{yyy}(r_i,\pi+\theta_i+\theta_j,r_j)]\cos 2(\pi+\theta_i+\theta_j)+S_{yxy}(r_i,\pi+\theta_i+\theta_j,r_j)\sin 2(\pi+\theta_i+\theta_j)\},
\end{aligned}
\tag{A.11}
$$

$$
\begin{aligned}
G_{\theta\theta\theta} = &\{\frac{1}{2}[S_{yxx}(r_i,\theta,r_j)+S_{yyy}(r_i,\theta,r_j)]-\frac{1}{2}[S_{yxx}(r_i,\theta,r_j)-S_{yyy}(r_i,\theta,r_j)]\cos 2\theta \\
&-S_{yxy}(r_i,\theta,r_j)\sin 2\theta\}+\{\frac{1}{2}[S_{yxx}(r_i,\theta_i+\theta_j,r_j)+S_{yyy}(r_i,\theta_i+\theta_j,r_j)] \\
&-\frac{1}{2}[S_{yxx}(r_i,\theta_i+\theta_j,r_j)-S_{yyy}(r_i,\theta_i+\theta_j,r_j)]\cos 2(\theta_i+\theta_j) \\
&-S_{yxy}(r_i,\theta_i+\theta_j,r_j)\sin 2(\theta_i+\theta_j)\}+\{\frac{1}{2}[S_{yxx}(r_i,\pi+\theta,r_j)+S_{yyy}(r_i,\pi+\theta,r_j)] \\
&-\frac{1}{2}[S_{yxx}(r_i,\pi+\theta,r_j)-S_{yyy}(r_i,\pi+\theta,r_j)]\cos 2(\pi+\theta)-S_{yxy}(r_i,\pi+\theta,r_j)\sin 2(\pi+\theta)\} \\
&+\{\frac{1}{2}[S_{yxx}(r_i,\pi+\theta_i+\theta_j,r_j)+S_{yyy}(r_i,\pi+\theta_i+\theta_j,r_j)]-\frac{1}{2}[S_{yxx}(r_i,\pi+\theta_i+\theta_j,r_j) \\
&-S_{yyy}(r_i,\pi+\theta_i+\theta_j,r_j)]\cos 2(\pi+\theta_i+\theta_j)-S_{yxy}(r_i,\pi+\theta_i+\theta_j,r_j)\sin 2(\pi+\theta_i+\theta_j)\},
\end{aligned}
\tag{A.12}
$$

$$G_{\theta r\theta} = \{-\frac{1}{2}[S_{yxx}(r_i,\theta,r_j) - S_{yyy}(r_i,\theta,r_j)]\sin 2\theta + S_{yxy}(r_i,\theta,r_j)\cos 2\theta\}$$
$$+ \{-\frac{1}{2}[S_{yxx}(r_i,\theta_i+\theta_j,r_j) - S_{yyy}(r_i,\theta_i+\theta_j,r_j)]\sin 2(\theta_i+\theta_j)$$
$$+ S_{yxy}(r_i,\theta_i+\theta_j,r_j)\cos 2(\theta_i+\theta_j)\} + \{-\frac{1}{2}[S_{yxx}(r_i,\pi+\theta,r_j) - S_{yyy}]\sin 2(\pi+\theta)$$
$$+ S_{yxy}(r_i,\pi+\theta,r_j)\cos 2(\pi+\theta)\} + \{-\frac{1}{2}[S_{yxx}(r_i,\pi+\theta_i+\theta_j,r_j)$$
$$- S_{yyy}(r_i,\pi+\theta_i+\theta_j,r_j)]\sin 2(\pi+\theta_i+\theta_j) + S_{yxy}(r_i,\pi+\theta_i+\theta_j,r_j)\cos 2(\pi+\theta_i+\theta_j)\} \quad \text{(A.13)}$$

List of Figures

Bibliography

[1] H. Neuber. Theory of stress concentration for shear-strained prismatical bodies with arbitrary nonlinear stress-strain law. *Trans. ASME, J. Appl. Mechanics*, 28(4):544550, 1961.

[2] G. Glinka. Energy density approach to calculation of inelastic strain stress near notches and cracks. *J. Engng Fracture Mechanics*, 22(3):485508, 1985.

[3] P. M. Blomerus and D. A. Hills. An efficient procedure for modelling limited plastic flow. *J. Mech. Engng.*, 212(8):731–740, 1998.

[4] T. Mura. *Micromechanics of Defects in Solids*. Martinus Nijhoff Publishers,Dordrecht, 1982.

[5] B. A. Bilby, A. H. Cottrell, and K. H. Swinden. The spread of plastic yield from a notch. *Proc. R. Soc.*, A272:304–314, 1963.

[6] A. Navarro and E. R. De los Rios. Short and long fatigue crack growth: A unified model. *Philosophical Magazine A*, 57(1):15–36, 1988.

[7] A. K. Head and N. Louat. The distribution of dislocations in linear arrays. *Aust. J. Phys.*, 8:1–7, 1955.

[8] N. I. Muskhelishvili. *Singular integral equations*. P. Noordhoff, Groningen, The Netherlands, 1953.

[9] D. A. Hills, P. A. Kelly, D. N. Dai, and A. M. Korsunsky. *Solution of cracks problems: the distributed dislocation technique*. Kluwer academic Publishers, Dordrecht, 1996.

[10] J. Dundurs. Elastic interaction of dislocations with inhomogeneities, in mathematical theory of dislocations. *Ed. T. Mura, ASME Pub., New York*, pages 70–115, 1969.

[11] S. P. Timoshenko and J. N. Goodier. *Theory of Elasticity*. McGraw-Hill, New York, 1964.

[12] J. Dundurs and T. Mura. Interaction between an edge dislocation and a circular inclusion. *J. Mech. Phys. Solids*, 12:177189, 1964.

[13] P. M. Blomerus and D. A. Hills. Modelling plasticity in finite bodies containing stress concentrations by a distributed dislocation method. *Proc. Instn. Mech. Engrs.*, 212:731, 1998.